Variable Stiffness Robotic Arm for Safe Human-Robot Interaction Using Layer Jamming

An Undergraduate Honors Thesis

Presented to The Department of Mechanical Engineering
The Ohio State University
In Partial Fulfillment of the Requirements for
Graduation with Distinction in Mechanical Engineering

by

Carter Hurd
March 19, 2017

Advisor: Haijun Su, Ph.D.

ABSTRACT

Soft robotics is an important frontier in robotics research. Due to the high compliance of soft robots, they can be extremely durable, less likely to damage the surrounding environment, and much safer for use around humans. These attributes are particularly desirable for "co-robots," or robots which share their workplace with people. However, soft robots lack the positional accuracy and load capabilities of traditional rigid robots. As such, there is a desire to create robots which combine the capabilities of traditional ridged robots with the safety of soft robots. Previous research has demonstrated a variable stiffness technology known as pneumatic-actuated layer jamming. The goal of this project was to build to a variable-stiffness robotic arm link utilizing this layer jamming technology to achieve the precision and load capabilities of a traditional robot and the safety of a compliant soft robot. To determine the best design for this arm, a test rig was set up to evaluate the stiffness of different layer jamming samples. Samples of various designs and materials were tested, and a positive relationship between the number of layers and the maximum stiffness was observed. A configuration with a high maximum stiffness was selected to give the robotic arm high load capabilities, and a prototype arm was built and evaluated. In the future, this type of robotic arm could safely work around humans by adjusting its stiffness in real time to ensure that it is in a safe, flexible state when contact with a person might occur.

ACKNOWLEDGEMENTS

This project was possible due to the support I had from others. I would like to thank my advisor, Dr. Haijun Su for his continuous commitment and support. Dr. Su has supported my robotics projects in the Design Innovation and Simulation Laboratory (DISL) for the past 3 years. This project would not have been possible without the materials and equipment of the DISL. Dr. Su's guidance has contributed to my success not only with this project, but with my career as well.

I would also like to thank Professor Xu Pei for his support of this project, and his guidance with the layer jamming process and fabrication techniques.

I would like to thank graduate student Yu She for giving his time to teach me how to use the laboratory equipment when I first started, and for his support and enthusiastic encouragement throughout this project.

And finally, I want to like to thank my parents for their moral support as I completed this undergraduate thesis amidst a very busy fourth year.

TABLE OF CONTENTS

LIST OF FIGURES

LIST OF TABLES

CHAPTER 1: INTRODUCTION

1.1 Soft Robots

Soft robotics is an important frontier of robotics research. Soft robots are typically constructed from materials such as textiles and elastomers, but can be made from any highly-compliant material. Due to their compliant nature and theoretically infinite degrees of freedom, flexible robots can be extremely durable, less likely to damage fragile payloads or harm humans, and more dexterous [3][4]. Soft robots are inertly more safe because of their compliance, and as such do not require careful control and environmental awareness to avoid damaging payloads or harming humans. Soft robots can also be less expensive, lighter weight, and easier to customize for different applications when compared to traditional robots [12].

There are some limitations associated with the high compliance of soft robots, however. One challenge with soft robotics is maintaining high positional accuracy. The inherit flexibility makes it difficult to know the exact position of the soft robot's appendages. The theoretically infinite degrees of freedom make applying traditional sensor setups such as encoders a challenge. Additionally, loads and quick acceleration simply cause a soft robot to flex. This prevents soft robots from matching the load-carrying capabilities and acceleration speeds of traditional rigid robots, which limits their potential uses.

1.2 Variable Stiffness Advantages

Because of the performance limitations of soft robots, there is interest in variable stiffness technologies. Robots with control over their stiffness could combine some of the advantages seen in soft robots with the performance of traditional rigid robots. For example, a robot capable of varying its stiffness can become more rigid when higher positional accuracy or load capabilities are needed, but can also become more complaint to prevent injuring surrounding humans or damaging the environment. The additional safety that variable stiffness allows for is of particular interest as robots which interact with humans become more common. For robots in assistive, rehabilitation, and domestic roles, safety is a critical design concern. This safety risk must be addressed before robots which work alongside humans can become more prevalent, and variable stiffness capabilities may be an important solution.

Existing research has shown that robotic arms designed with greater compliance are less likely to cause injury to humans [1] [14]. Furthermore, models of how to control the motion of such a variable-stiffness robot arm have been explored. Figure 1 shows one proposed control scheme in which the stiffness of a variable-stiffness robotic arm is reduced when the velocity is high, and increased when the velocity is low. This type of control would reduce the potential impact injuries when the robot is moving quickly, while still allowing for positional accuracy before and after the movement. The higher stiffness at either end of the movement also helps with the acceleration and deceleration of the appendage.

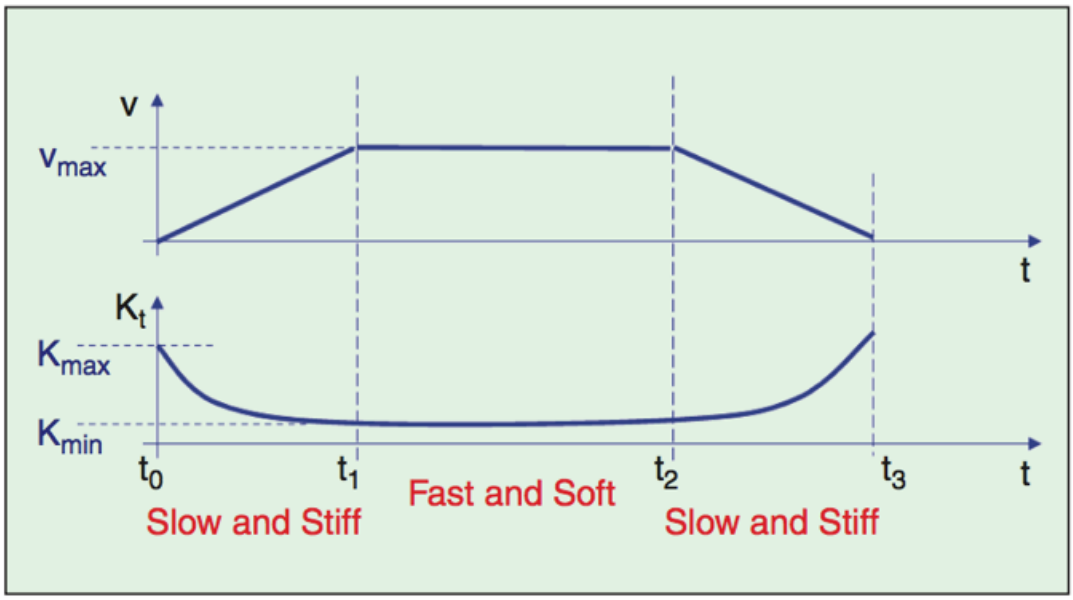

Figure 1: Proposed control of a rest-to-rest movement using a variable stiffness robot arm [1]

1.3 Variable Stiffness Technologies

Several variable stiffness technologies have been explored in past research. In the Design Innovation and Simulation Laboratory, a robot arm link was built with active stiffness control. The robot link consists of two parallel beams, and the stiffness is controlled by altering the shape of these beams. Figure 2 shows the maximum stiffness and maximum compliance modes of this robot arm. Figure 3 shows the mechanical linkage mechanism used to actively control the curvature of the two parallel beams. This design allows for a stiffness change of 3.6 times [1]. Testing of this variable stiffness robot link showed a significant reduction in head injury criteria (HIC) when the beam is in its more compliant mode [1].

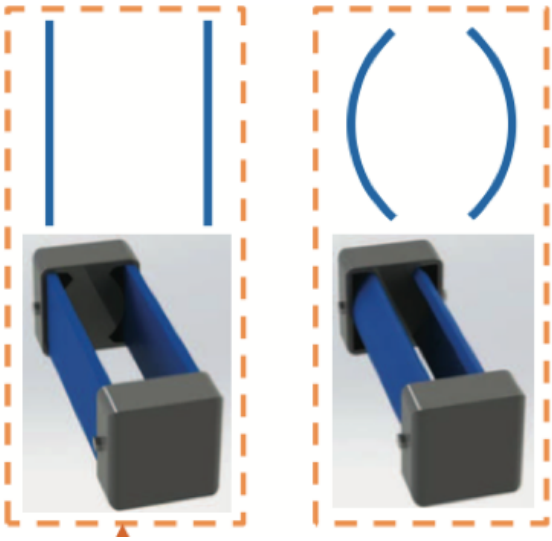

A. **B.**

Figure 2: Variable stiffness robot arm link [14]
A. Straight beams (compliant)
B. Curved beams (stiff)

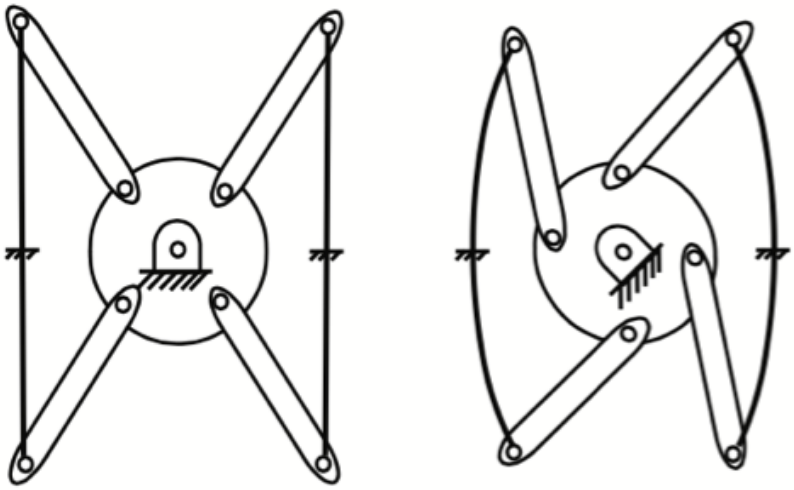

A. **B.**

Figure 3: Stiffness control linkage mechanism [14]
A. Straight beams (compliant)
B. Curved beams (stiff)

This mechanical approach to a variable-stiffness has safety advantages when compared to a traditional rigid robot, but it requires a mechanism to actively alter the beam shapes. This linkage mechanism has some disadvantages, as it adds complexity. The additional actuation motors, linkages, and other components increase the price of such a

variable stiffness robot arm, would make it more difficult to mass produce, and introduce new points of failure.

One variable stiffness method which does not require additional motors and linkages uses low-melting-point materials. Both low-melting-point polymers and alloys can be used, although the heating of polymers is significantly slower due to their lower thermal conductivity [2]. One variable stiffness configuration using low-melting-point alloys imbeds the alloy within an encapsulation layer made from silicon or another soft material. When current is run through the alloy, the temperature increases and it becomes a liquid, causing the stiffness of the structure to decrease. This configuration is capable of stiffness changes of greater than 25 times [8][2]. While very high stiffness changes are possible utilizing low-melting-point materials, they cannot change stiffness as rapidly as other methods. The speed at which these materials cool to their maximum stiffness state is too slow to allow for real-time stiffness change during the motion of a robotic appendage. Additionally, experiments using low-melting-point alloys suggest that this variable stiffness method is not durable enough to handle high loads and impacts. The alloys used are susceptible to fracture at low strain amounts when in their solid state, in some cases as low as 0.2% strain [2].

Magnetorheological materials are another variable stiffness technology. These materials are imbedded with ferromagnetic particles. When a magnetic field is applied, the positions of the imbedded particles change, altering the properties of the material. Many Magnetorheological materials are viscus fluids, but magnetorheological elastomers are solid. These magnetorheological elastomers are capable of variable stiffness. This

technology has been used to adjust the spring constant of vibration absorbers in real time for better vibration isolation [7][9]. However, at this time the technology is not ideal for structural parts. Existing magnetorheological elastomers are usually made from a soft elastomer such as silicon imbedded without iron particles (70% mass ratio in one study) [9]. The elastomer must be extremely flexible for the ferromagnetic particles to be able to shift within it. This flexibility makes these materials less suited for use as a major structural part of a robotic appendage. Additionally, the electromagnets used to activate magnetorheological elastomers would pose packaging difficulties if the material was implemented on a large, moving part of a robot.

Jamming structures are another variable stiffness method that has been explored in past research. Jamming structures consist of a sealed volume, filled with a medium, usually either a granular material, or sheets of material. When sheets are used, the technique is known as layer jamming. When a vacuum pump is used to remove the fluid from the airtight volume, the negative air pressure presses the particles or sheets together, increasing the friction between them. This increased friction restricts the particles or sheets from moving relative to each other, which causes the stiffness of the structure to increase. The sealed volume goes from being flexible to rigid, and a continuum of stiffness values between the two extremes can be achieved by varying the pressure. [6][11]

Robots using jamming structures have demonstrated many of the advantages of soft robots combined with the capabilities of traditional, rigid, robots. A robotic grasping appendage using jamming can safely handle a delicate object when the stiffness is low,

but can also lift large loads when the stiffness is increased [11]. A manipulator using jamming for minimally invasive surgery can assume a flexible state for insertion without accidental injury, but can then become stiff to achieve the required positional accuracy [13]. The technology has also been used for mobile robot locomotion [5]. Layer jamming specifically has been used in applications requiring high strength, such as a stool which can support a person's weight as shown in Figure 4 [10].

Figure 4: Layer Jamming Stool [10]

1.4 Thesis Objectives

The purpose of this thesis is to design a variable stiffness robot link for safe human-robot interaction. The variable-stiffness robotic links which have been developed at the Design Innovation and Simulation lab use mechanical mechanisms to adjust the stiffness. This thesis aims to investigate an alternative method of variable stiffness which does not require a mechanical mechanism. Of the variable stiffness technologies, layer

jamming was selected for this application. Layer jamming is more suitable for the loads which a robotic arm link will experience than the other non-mechanical variable stiffness technologies that were investigated.

The first objective in applying layer jamming to a robot link was to investigate layer jamming techniques and work on improvements to increase the maximum stiffness. The greater the maximum stiffness of the laminar, the better the robot link's ability to match the performance characteristics of a traditional rigid robot. Test laminar were constructed, and testing was done to evaluate the stiffness while using different numbers of sheets, different materials, and different imbedded supports.

The second objective of this thesis was to design and construct a prototype robot link and evaluate the prototype's stiffness behavior in different configurations. The performance of this variable stiffness link was then compared with the performance of the mechanical-mechanism actuated link.

1.5 Overview of Thesis

This thesis in composed of six chapters. Chapter 1 introduces the advantages of variable stiffness in robotics, reviews the variable stiffness technologies, and describes the objectives of this thesis. Chapter 2 discusses the initial layer jamming test setup and Chapter 3 discusses the results of this initial testing. Chapter 4 discusses the design of the prototype robot link. Chapter 5 presents and discusses the test results of the prototype robot link. Chapter 6 concludes the lessons learned from the construction and testing of this layer jamming robot link

CHAPTER 2: LAYER JAMMING METHOD FOR VARIABLE STIFFNESS

This chapter discusses the initial investigation of layer jamming as a method for variable stiffness. Section 2.1 describes the design and construction method of a single beam laminar used for the initial investigation. The laminar has several configurations with different layer numbers and center support designs. The deflection test used to evaluate the stiffness of this single beam laminar is described in Section 2.2.

2.1 Design of Single Beam Laminar

An initial investigation of layer jamming had to be completed before it could be applied to a robot arm link. For this, a reconfigurable laminar was made, and the stiffness properties of this beam-shaped laminar was tested. The components of a layer jamming laminar are shown in Figure 5. The exterior of the laminar is sealed with a flexible air tight material. Within the volume are the layers. Optionally, there can be a center support to help to self-center the laminar after a deflection. This center support has not been used in other layer jamming research, however for this application self-centering is desired. An external vacuum pump applies negative air pressure to the volume via a 3mm diameter hose.

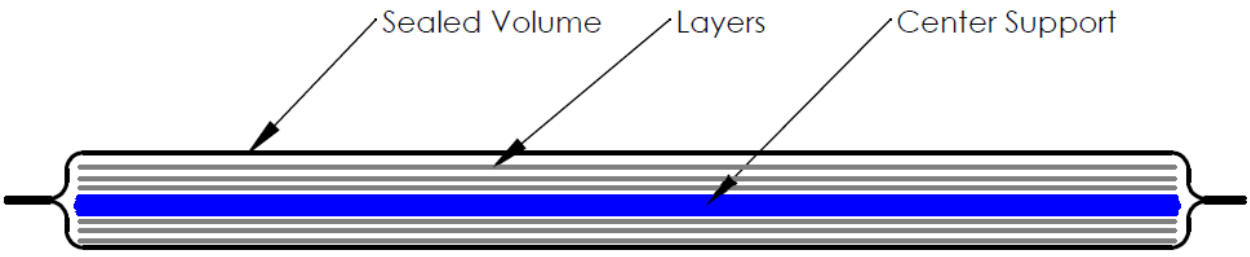

Figure 5: Components of Layer Jamming Laminar

For the initial layer jamming investigation, the laminar exterior was 12cm x 26cm in size. This was representative of the expected robot arm link size, and constrained by the print volume of the 3D printer available to print the center support. The sealed exterior was made from two identical sheets cut out of a commercially available food vacuum bag. Figure 6 shows how three sides of these two sheets were lined up and heat sealed to form a volume open on one side. The one open side allowed for different layers to be slid in and was sealed using a clamp discussed in subsequent pages. For the heat-sealed sides, a soldering iron on low heat was run along 5mm from the edge until the two sheets melted together.

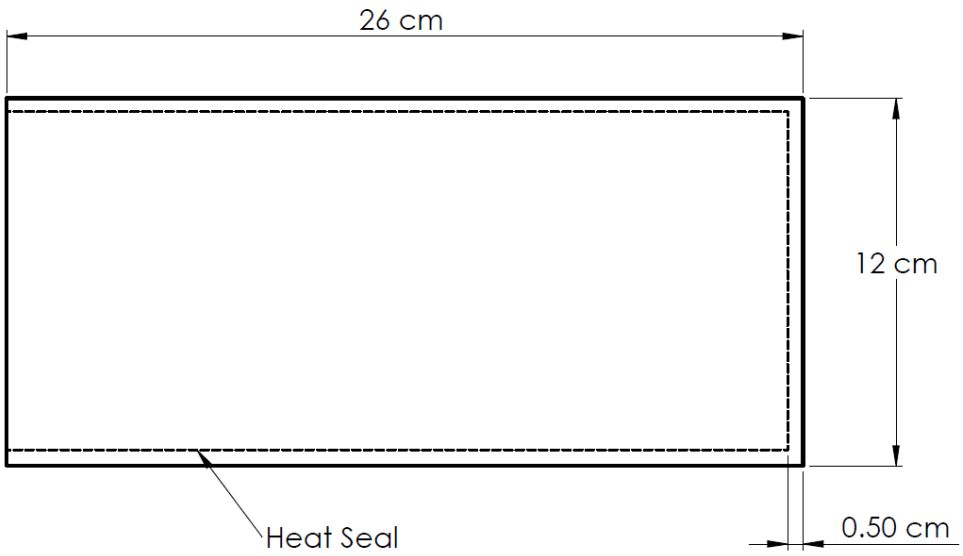

Figure 6: Heat-Sealed Vacuum Bag

The layers within this sealed volume were sheets of Dura-lar polyester 0.005" matte film. Matte polyester film was chosen for its minimal thickness while still being resistant to creasing and wrinkling. The minimal thickness allowed for many layers, while the durable wrinkle-resistant properties of the polyester film insured that the layer

jamming effect would not be minimized by the layers stretching or tearing when in tension, or wrinkling under compression.

Two configurations were used for the layers, traditional and interlocked. The two configurations can be seen in Figure 7. With the interlocked configuration, the short sides of every other sheet were joined at one end, and the other sheets were joined at the opposite end. In Figure 7 the red area indicates the location where the matte film sheets were attached to each other using super glue. In the configurations with a center support the ends of the sheets were also attached to the center support. This interlocked configuration was fabricated to test if limiting the slip between the sheets would improve the maximum stiffness of the laminar. For the traditional configuration, the layers were 10cm x 21cm. For the interlocked configuration, the layers were slightly shorter at 10cm x 19cm to accommodate the adhesive area at the ends.

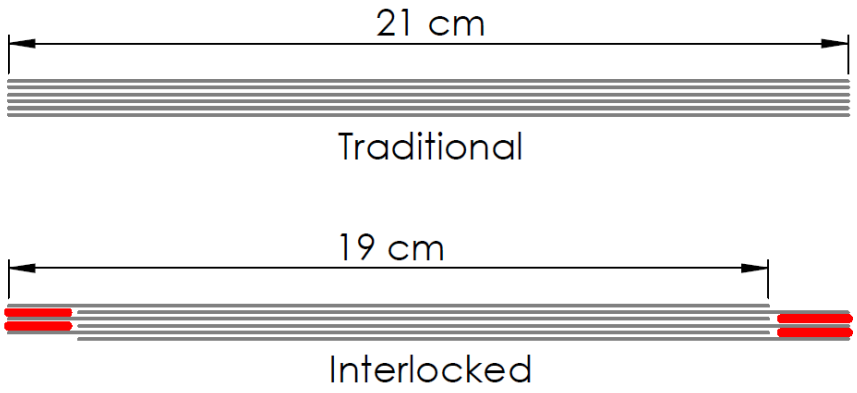

Figure 7: Traditional vs. Interlocked Layer Configurations

Center supports of three different designs were made for the initial layer jamming investigation. These were 3D printed out of ABS. Figure 8 shows the design of these

center supports. The 10mm wide center support had flexible sections along its length so that it could still bend despite the width. Figure 9 shows a close view of one of the flexible sections of the 10mm wide center support. The design of the center support with holes in it was intended to increase the friction against the polyester sheets when compared to the solid center support.

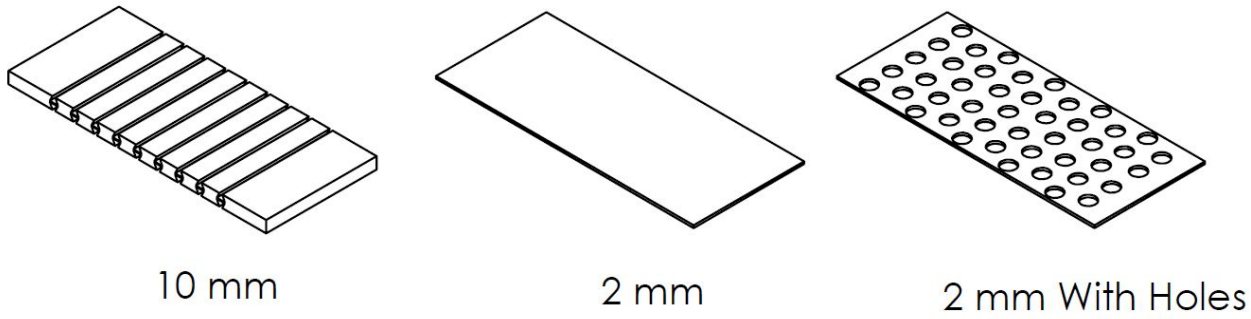

Figure 8: Center Support Designs

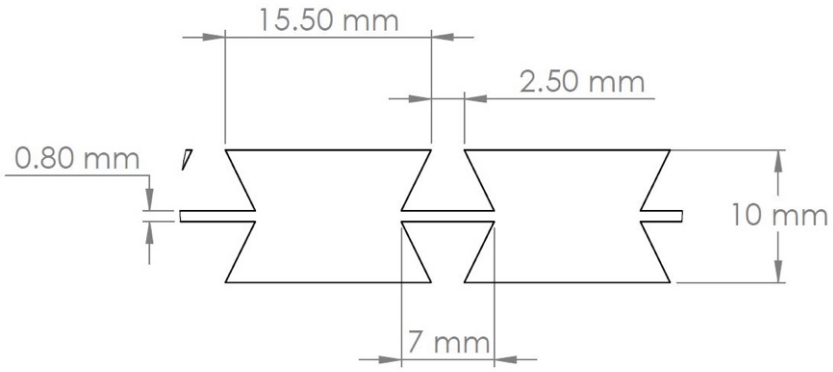

Figure 9: 10mm Center Support Section View

A custom silicon clamp was used to seal the one open side of the laminar volume. The design of this clamp can be seen in Figure 10. Sealing the fourth side with this clamp

instead of permanently sealing the vacuum bag allowed for easy changes to the laminar within the volume. The silicon conformed to the pneumatic hose, providing an airtight seal. In addition to sealing the vacuum bag and hose connection, this clamp provided a secure mount with which to hold one end of the laminar during deflection testing. The two exterior sides of the clamp were laser cut from ¼" acrylic, while the two interior sheets were made from Ecoflex 00-30 silicon. For thicker laminar samples, such as ones with the 10mm wide center support, an additional silicon spacer was added. A 3D printed ABS mold was used to cast the silicon parts. Four bolts were used to secure the clamp onto the end of the laminar.

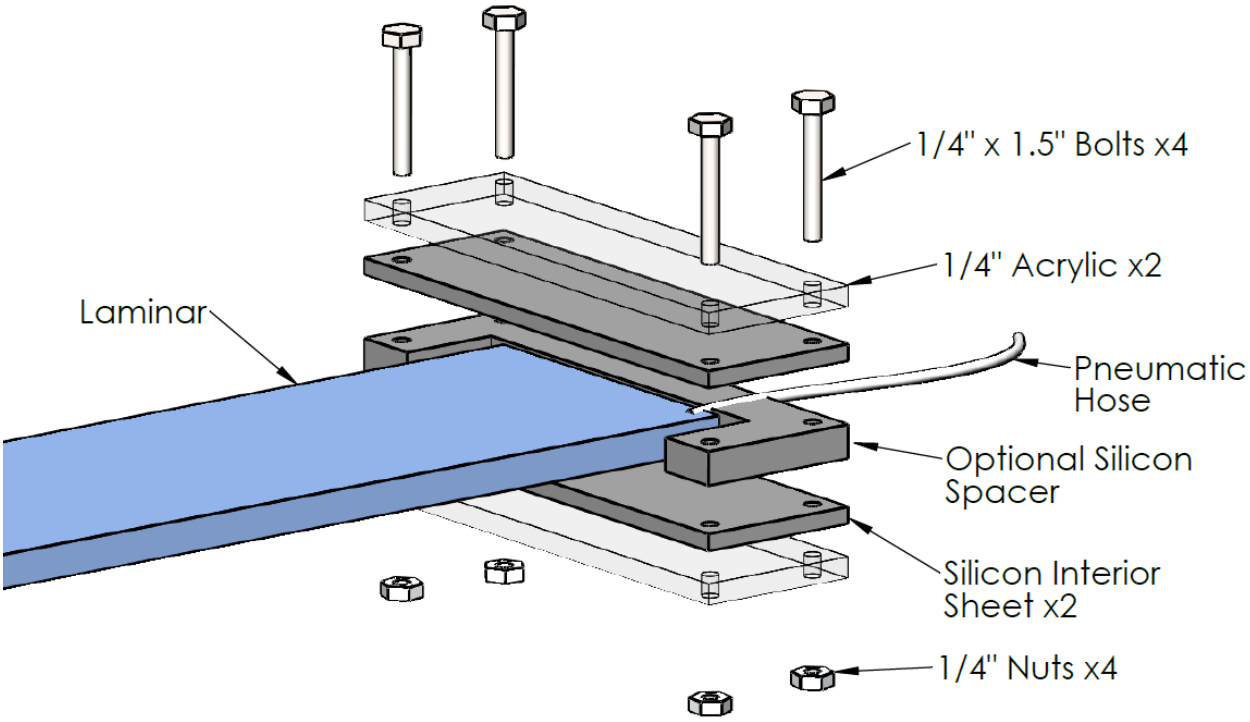

Figure 10: Sealing Silicon Clamp

2.2 Single Beam Deflection Test Setup and Procedure

A force vs. deflection test was used to compare the stiffness of the test laminars. Figure 11 shows the test setup. A PASCO PS-2189 high resolution force sensor was used with a PASCO Spark PS-2008A to measure and display the deflection force. The force sensor was mounted to a Mark-10 linear slider rig. One end of a SpiderWire .20mm Dia Dyneema cord was tied to sensor hook of the force sensor and the other end tied to a 3D printed hook that attached to the end of the laminar opposite the silicon camp. The end of the laminar with the silicon clamp was secured to the table using a vice, and the laminar was positioned to be perpendicular to the Dyneema cord. The Mark-10 linear slider rig was equipped with a Mitutoyo 12" digital caliper, which was used to measure the deflection amount. An external vacuum pump, RobinAir model BTA48RA, was attached to the vacuum hose of the laminar, and a pressure gauge was used to monitor the negative pressure applied to the laminar.

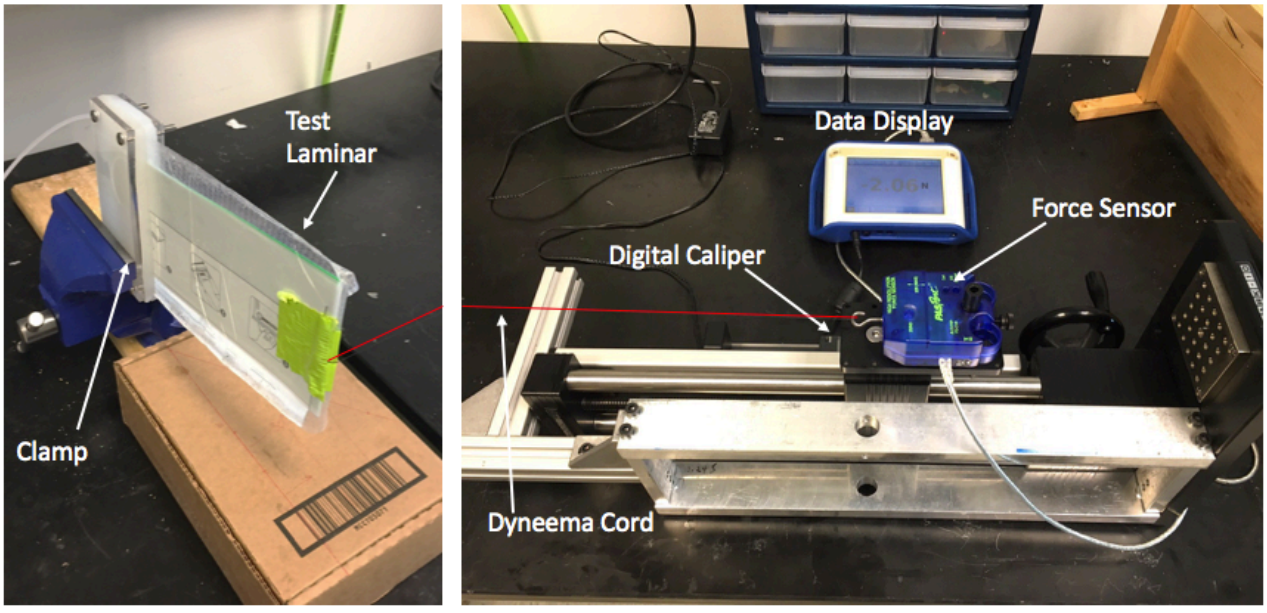

Figure 11: Deflection Test Setup

Before the testing, the force sensor was zeroed without the Dyneema cord. At the start of each deflection test, the laminar was centered without any tension from the cable and the pressure was adjusted to the intended amount. Then the linear slider rig was moved until the cord was taught, but no deflection of the laminar had occurred. At this position the digital caliper on the slider was zeroed. To deflect the sample, the handle of the linear slider rig was rotated at a constant rate counter clockwise, for a deflection speed of approximately 1.6 mm/s. There were no pauses during the deflection of the sample. After deflection, the handle of the linear slider rig was rotated in the other direction, and the slider rig returned to zero at the same rate. The values displayed on the PASCO Spark were recorded at given distance increments during the deflection and return. For different tests the sample was deflected by different amounts.

CHAPTER 3: RESULTS OF INITIAL LAYER JAMMING INVESTIGATION

This chapter presents and discusses the results of the force vs. deflection tests using the single beam laminar. Section 3.1 presents the consistency tests used to validate the deflection test setup. Section 3.2 compares the different laminar configurations and selects a center support design with the highest stiffness values. Section 3.3 shows the force vs. deflection curves at different pressures. Section 3.4 discusses the stiffness contribution of the tension and compression laminar layers.

3.1 Consistency Tests

Before different samples of the laminar were tested, the consistency of the test setup and procedure was first checked. A laminar with 8 sheets in the traditional layout and a 10mm center support beam was used for the consistency tests. The sample was deflected three times to 12mm at a low negative pressure of 10cmHg, three times to 12mm at 60cmHg, and three times to 25mm at 60cmHg. The results are shown in Figure 12 and Figure 13.

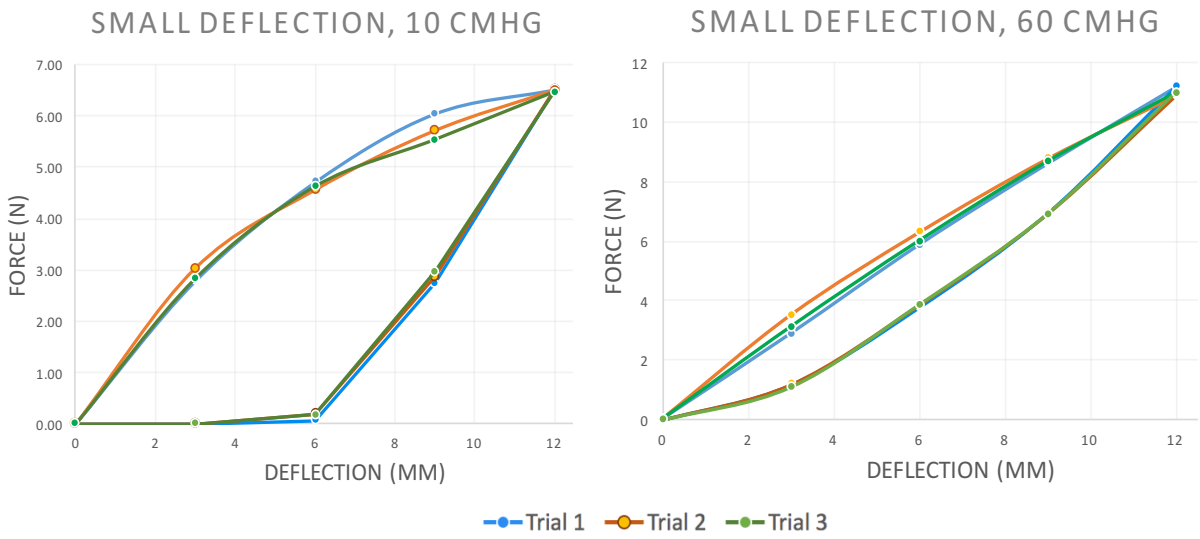

Figure 12: 12mm Deflection Consistency Tests

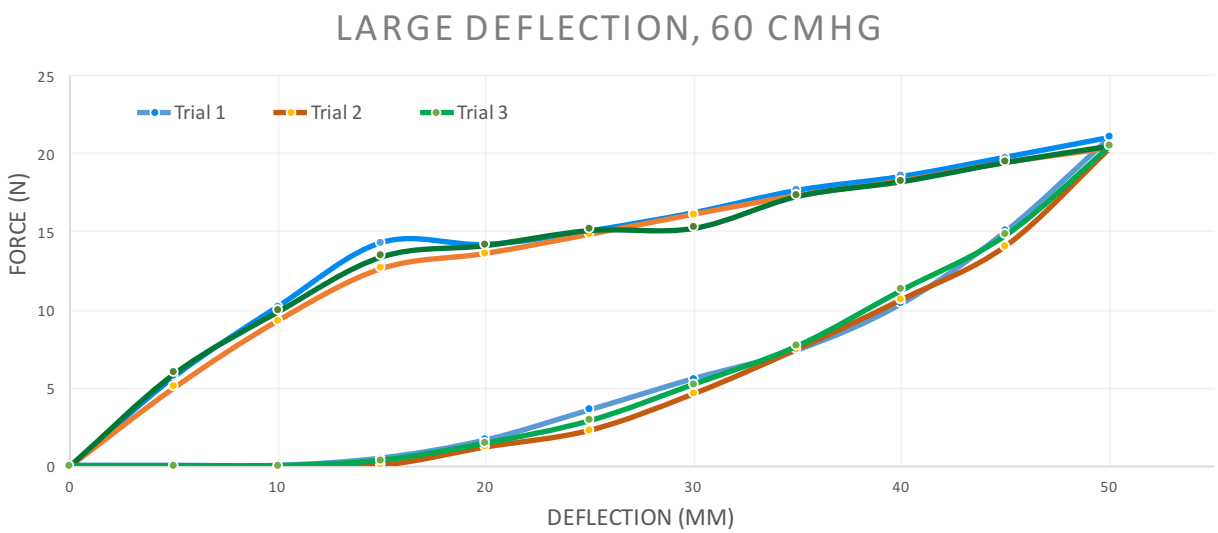

Figure 13: 50 mm Deflection Consistency Test

The force vs. deflection curves were consistent between the trials. The standard deviations of the maximum measured forces were calculated for each of the three scenarios. For the low and high pressure small deflection tests, the standard deviations where σ=0.02N and σ=0.145N respectively. The maximum pressures from the large deflection test had a standard deviation of σ=0.35N. These standard deviations were very small compared to the effect that deflection amount and pressure amount had on the measured force. As such, the test rig and procedure was determined to be reasonably consistent for comparing the performance of different laminars.

3.2 Laminar Configuration Assessment

To determine the center support configuration best for the robot arm link, a deflection test was run on numerous laminar configurations. Each laminar configuration was tested at zero pressure and at the maximum negative pressure possible with the vacuum pump,

70cmHg. Maximum and minimum deflection force was found to correspond to the maximum and minimum pressure for all samples. The samples were each deflected to 100mm, and the resulting force was recorded. Table 1 shows the results. The traditional configuration was used for the layers for the samples in Table 1.

Table 1: Comparison of Center Support Configurations

Center Support	Number of Sheets	Force (N) at Deflection of 100mm	Δ Force (N): Max force-Min force	Maximum Stiffness Change
None	10	1.65	1.59	27.5 x
None	30	5.6	5.41	29.4 x
None	40	6.81	6.60	32.4 x
None	50	8.02	7.69	24.3 x
Solid 2mm ABS Centered	10	4.25	3.71	7.8 x
Solid 2mm ABS Compression Side	10	3.54	3.00	6.8 x
Solid 2mm ABS Tension Side	10	3.21	2.74	6.5 x
Solid 2mm ABS	4	2.31	1.69	3.6 x
Solid 2mm ABS	30	6.20	5.47	8.5 x
Solid 2mm ABS	40	8.60	7.68	9.3 x
2mm ABS Holes	4	1.19	0.98	5.6 x
2mm ABS Holes	10	2.89	2.62	10.7 x
2mm ABS Holes	30	5.90	5.30	9.8 x
2mm ABS Holes	40	7.90	6.01	8.5 x
10mm ABA	4	25.00	21.90	8.1 x
10mm ABS	10	29.00	25.13	7.5 x

The grey rows of Table 1 show only laminars with 10 sheets of polyester matte film. From these rows the effects of the different center supports can be seen. The laminar with the 10mm center support had the largest maximum deflection force by a significant margin: 29N compared to 4.25N of the next largest. The laminar with no center support

had the smallest maximum deflection force. The deflection force of the laminar with the 2mm support with holes in it was less than the deflection force of one with the 2mm solid support. For layer jamming to be useful in a variable stiffness robot arm link, the maximum stiffness configuration must be comparable to the performance of a rigid robot link. Thus, a high maximum stiffness and high maximum deflection force is desired. In this respect the wide 10mm support was the most ideal of the 3 tested supports for this application. A high stiffness change is also preferred, but is not useful if the maximum stiffness is not sufficient for the robot link's use. Using a center support was found to reduce the maximum possible stiffness change. The laminar with no center support had a stiffness change of 27.5 times, while the laminar with the 10mm center support had a stiffness change of 7.5 times. For this application, the tradeoff of a lower stiffness change percentage is worth it for the greater maximum stiffness possible with a wide center support.

Table 1 also addresses the ideal position of the center support. Until now it has been assumed that the center support was placed with an equal number of film sheets on either side. However, the self-centering effect, where the beam returns to the zero-displacement position on its own after a deflection, does not depend on the location of the support. The center support can also be placed on either side of the film sheet layers. This scenario is shown in rows six and seven in Table 1. When the support was placed on the tension side or the compression side of the laminar, the maximum deflection force was lower than when the support was placed in the center. The percent stiffness change

and Δ force was also lower. It was determined that the center location is ideal for this application.

These initial results also show the effect of different layer numbers. Samples with a greater number of layers had a greater maximum deflection force. The relationship between maximum deflection force and layer number was nonlinear. To determine the effect of the layer configuration, deflection tests were done using the 10mm center support and the interlocked configuration. The comparison of these results with the traditional sheet configuration are shown in Table 2.

Table 2: Traditional vs. Interlocked Configurations

Center Support	Layer Configuration	Number of Sheets	Force (N) at Deflection of 100mm	Δ Force (N): Max force-Min force	Maximum Stiffness Change
10mm ABA	Traditional	4	25.00	21.90	8.1 x
10mm ABS	Traditional	10	29.00	25.13	7.5 x
10mm ABS	Interlocked	4	30.00	26.80	9.4 x
10mm ABS	Interlocked	10	36.00	32.20	9.5 x

The interlocked layer configuration performed better than the traditional layer configuration. The maximum deflection force was 20% and 24% greater for the 4 sheet and 10 sheet tests respectively. The maximum stiffness change and Δ force was also greater with the interlocked layers. This result is likely due to the way the interlocked configuration prevents slip between the layers at the edge of the laminar. With the traditional configuration, the layers at the ends are free to slide relative to each other. When the laminar is deflected, the stresses are greatest at the base where the laminar is clamped. The sheets in this end can slip relative to each other, causing deflection to

occur. This is not possible with the interlocked configuration. For deflection to occur with the interlocked configuration, slip must happen over the entire length of the layers. The interlocked configuration was selected for use with the robot link, and was used for all following tests.

3.3 Single Beam Pressure Tests

The behavior of the layer jamming laminar over a range of pressures was investigated next. A laminar with a 10mm wide center support and 8 layers in the interlocked configuration was used. Figure 14 shows the force vs. deflection curve of the sample deflected to 50mm at a five different pressure levels.

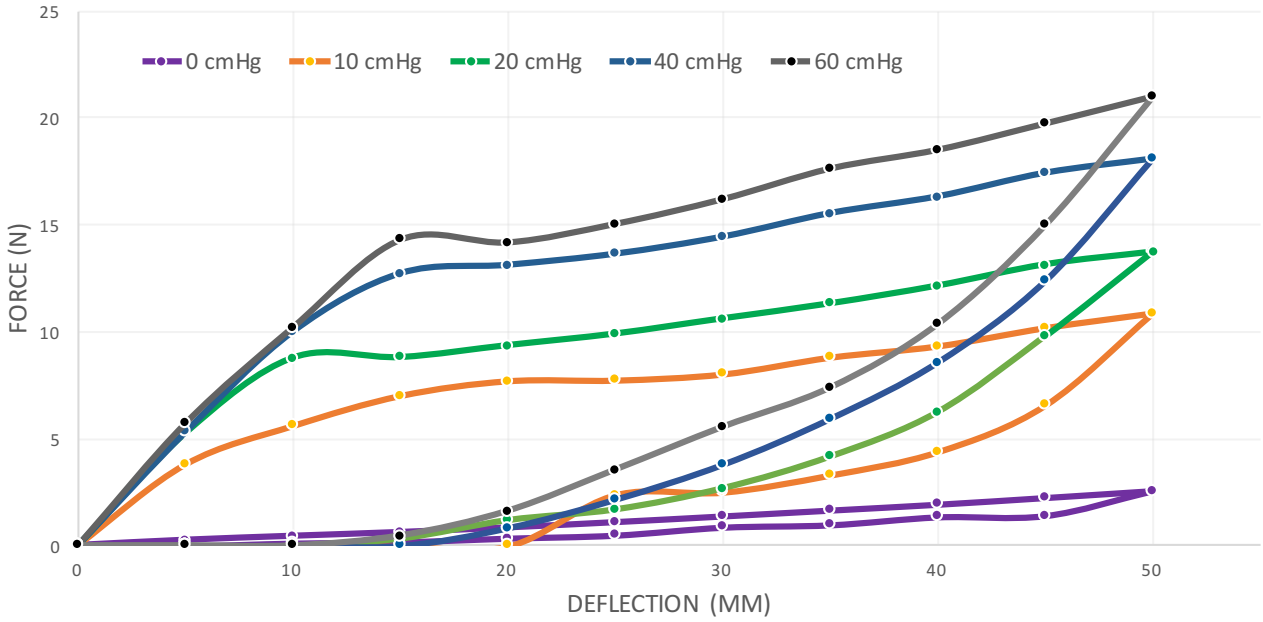

Figure 14: 50mm Deflection Single Beam Pressure Tests

The curves shown in Figure 14 reveal the deflection properties of the layer jamming laminar. After 50mm of deflection the laminar does not fully return to the zero position when pressure is above zero. Lower pressure tests did not get closer to returning to zero,

either. All tests with the pressure above 0 cmHg stopped returning to zero around the 15mm deflection position and remained there until the pressure was removed. When pressure was removed the laminar would then self-center. The layers likely slid relative to each other during the deflection, and remained in their new positions after sliding while the laminar was jammed with a pressure above zero. When the pressure was removed the friction forces between the layers was no longer significant, allowing the center support to return the laminar back to the zero position.

An interesting feature seen in the force vs. deflection curve of Figure 14 is the slip point. The slip point occurs around 10mm to 15mm on the load curves where the slope of the force vs. deflection curve drops off. At greater pressures the slip point occurred at greater force and displacement. Before this point the layers are not sliding relative to each other, and the laminar deflects in a way similar to a solid beam. After this point the layers begin sliding and the resistance to deflection is determined by the kinetic friction between the layers instead of the greater static friction. This causes the reduction in stiffness, represented as a reduced slope.

The slip point is important for a robot link application. When the robot link is in its maximum stiffness mode, positional accuracy and load capabilities are desired. For this maximum-stiffness operation, the laminar of the robot link should never deflect past the slip point. If the beam regularly deflected past the slip point, it might not return to center, and the position of the link end would be unpredictable, and positional accuracy would be lost. This would make it unable to match the performance of a rigid robot link. For this reason, it is desirable for the slip point to occur at a large force, that way the

robot can accelerate quickly and move large loads when in the maximum stiffness mode without slip occurring. To investigate what the force vs. deflection looked like before the slip point, a second test was done with 12mm deflection instead of 50mm. The results of this test can be seen in Figure 15.

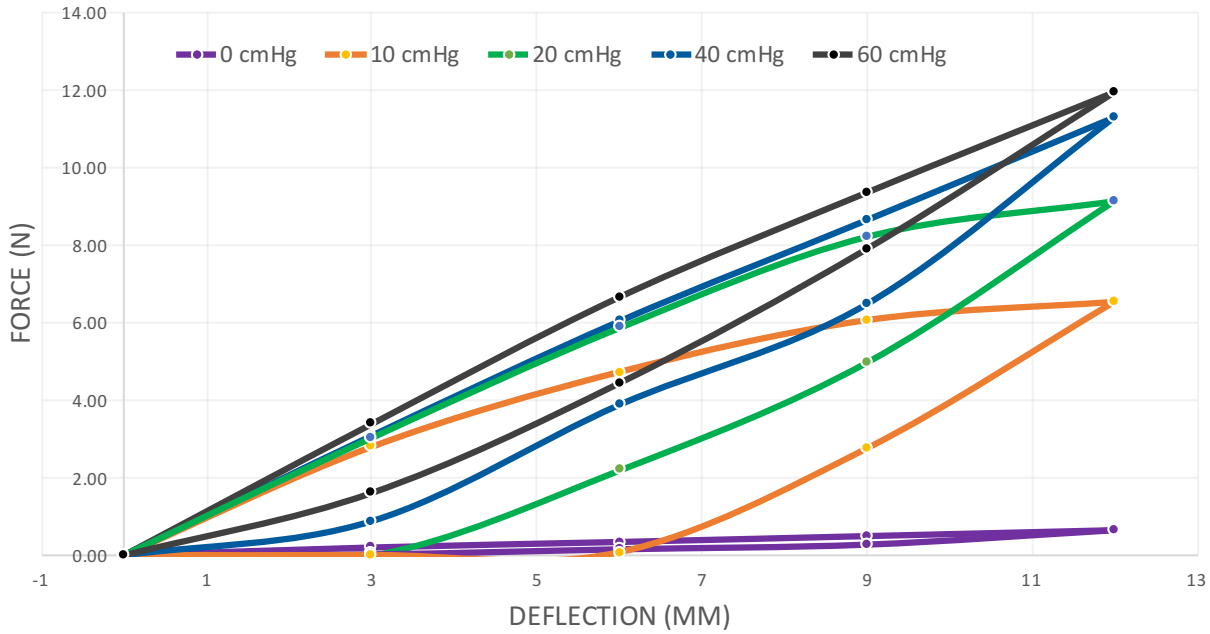

Figure 15: 12mm Deflection Single Beam Pressure Tests

After being deflected 12mm, the laminar returned to the zero position at every pressure except for 10 cmHg and 20 cmHg. At these pressures the laminar returned to 3mm before stopping. Even with this smaller deflection, some slip or settling did occur between the layers. This is evident because the unloading curve did not match the loading curve for any of the pressures. This hysteresis is one of the ways this laminar differs from a solid beam. The higher pressures had less hysteresis and more linear force vs. deflection curves, likely because the higher pressure increased the friction forces between the layers and limited slip from occurring. Despite the hysteresis, the laminar

sample did return to zero at the higher pressures. This indicates that when the deflection amount is low, the laminar will not permanently deflect and positional accuracy will not be lost.

For layer jamming to be implemented in a variable stiffness robot, it would be best if the stiffness curve were predictable as pressure is varied. This would allow for predictable control over the link's stiffness. A pressure change test was done to see how the force vs. deflection curves from Figure 15 compared to a laminar whose pressure was altered mid-test. The results of this pressure change test can be seen in Figure 16. The laminar was deflected at 60cmHg, then the pressure was reduced to 20 or 0 cmHg, after which the beam was unloaded. The return curves after the pressure was reduced mid-test are shown in blue and red in Figure 16. For comparison, the 20c mHg and 0 cmHg return curves from the constant-pressure test of Figure 15 are also shown on Figure 16.

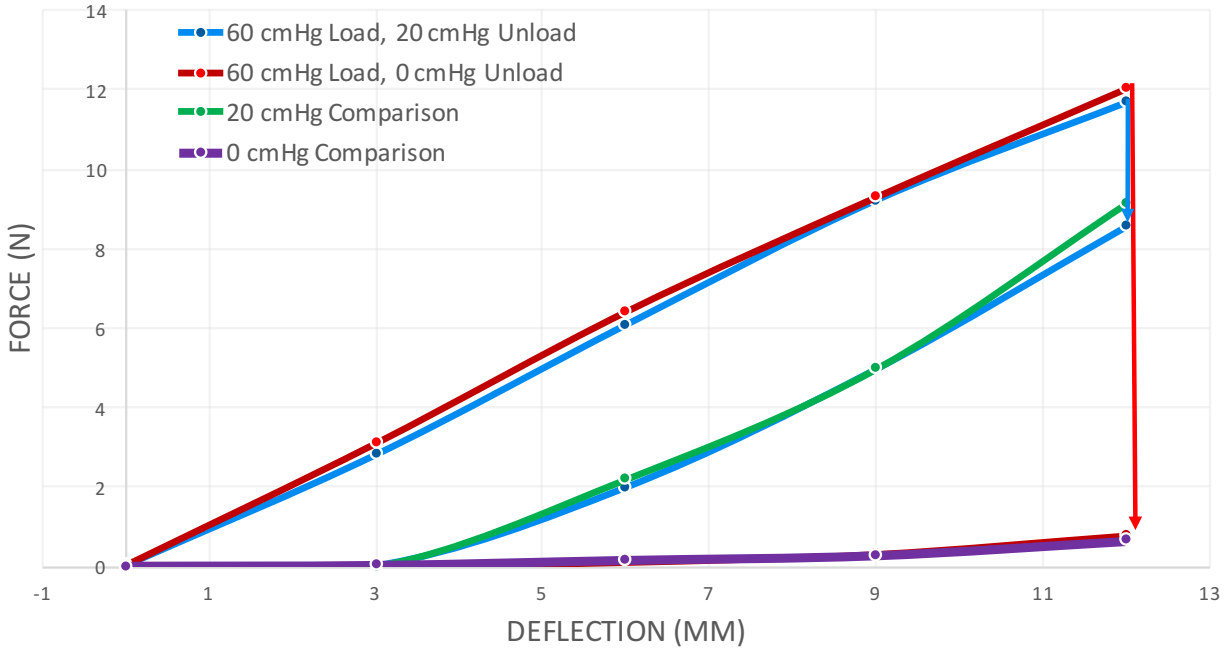

Figure 16: Pressure Change Test

As can be seen in Figure 16, the return curves of the sample whose pressure was altered mid run match the return curves of the samples already at 0 and 20 cmHg. This means that for conditions where slip has not occurred, the laminar's stiffness is predictable even if the pressure is altered while the laminar is deflected. In a robotic application where the pressure is being actively controlled in real time, the laminar's past pressure value will not impact its current stiffness value.

3.4 Tension vs. Compression Layers

During testing it was hypothesized that the sheets on the tension side of the laminar contributed more to the stiffness. To test this, the tension side sheets were removed from the laminar and it was deflected at 20 cmHg and 60 cmHg. Then the sample was flipped so there were no compression side sheets, and the experiment was repeated. The results were compared to the results from Figure 15. Figure 17 indicates the two sheet types: compression sheets are shown in green and tension sheets are shown in red. Figure 18 shows the results compared to the results from Figure 15 with all the sheets.

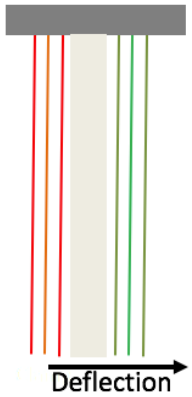

Figure 17: Compression vs. Tension Layers
Red: Tension Layers
Green: Compression Layers

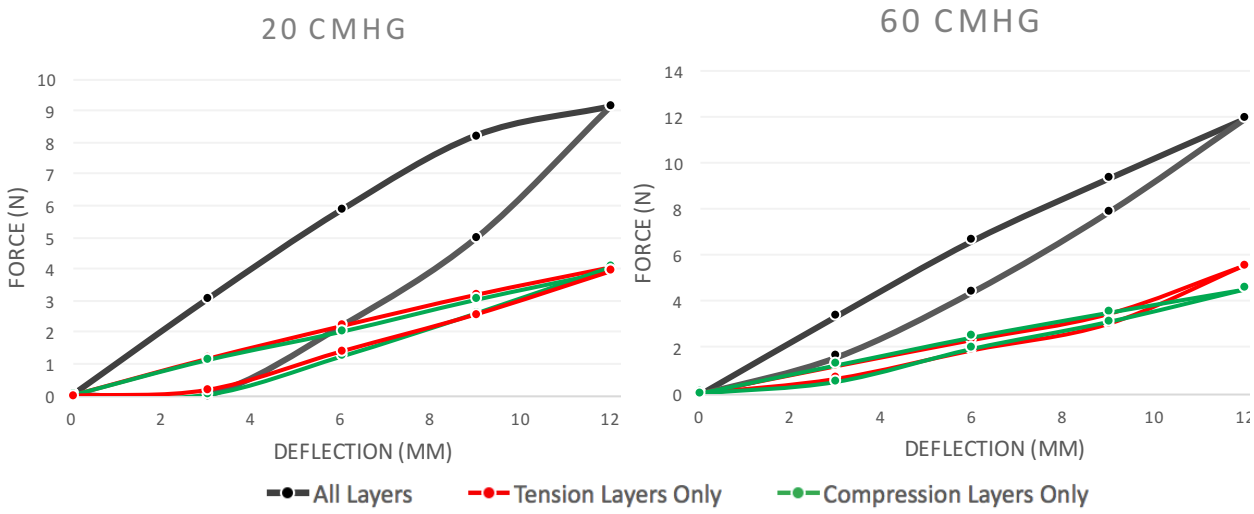

Figure 18: Tension vs. Compression Tests

Figure 18 shows that the contributions of the compression layers were comparable to the contributions of the compression layers. Neither side contributes a significant majority of the laminar's stiffness. Also notable is that all three laminars did not return fully to 0 mm deflection in the 20 cmHg test. This suggest that slip is occurring between both the compression side layers and the tension side layers in scenarios where the laminar does not fully return to zero.

CHAPTER 4: DESIGN OF ROBOT LINK

This chapter discusses the design and analysis of a prototype variable stiffness robot link utilizing layer jamming. Section 4.1 describes the design goals and discusses the prototype link design and assembly. Section 4.2 covers the analysis of the robot link. Section 4.3 proposes and tests a method for equipping the robot link with deflection feedback.

4.1 Prototype Robot Link Design

After investigating the properties of layer jamming using a single laminar, a robot link was designed. There were several goals for the prototype variable stiffness robot link. First, the max stiffness was to be greater than the stiffness seen in single laminar tests to better replicate a rigid robot. Second, the robot link was to have a more permanent sealing method for the laminar's exterior vacuum bag, without removing the ability to alter the number of layers when necessary. The silicon clamp used in the single beam tests was ideal for rapid changes to the laminar, but a more robust clamp on the laminar was desired for the prototype robot link. Third, the prototype link was to support large forces in the vertical direction without deflection, such that it could be used on a load carrying robot arm.

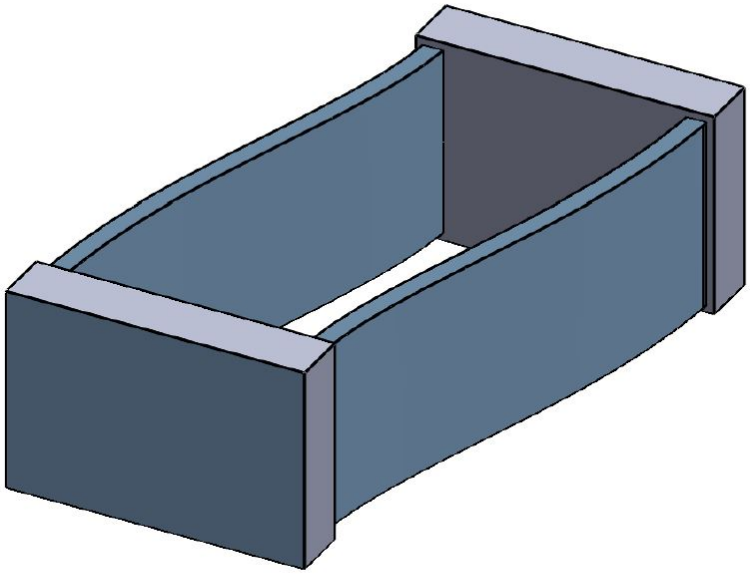

Figure 19: Dual Beam Configuration

To meet these requirements, a dual parallel beam configuration was selected. Figure 19 shows this configuration in a deflected state. This dual beam configuration has several advantages over a single beam. It meets the first requirement, as it has a higher resistance to deformation than a single beam. This is not only due to the dual laminar, but also due to the end constraints imposed on the deflecting end of the laminars. For a single cantilevered beam with a force applied at the end, the Force/Deflection can be seen in Equation 1. Although a layer jamming laminar is not a solid beam, it is approximated as such for comparing a single beam configuration to a parallel beam configuration.

$$\frac{F}{\delta} = \frac{3EI}{L^3} \tag{1}$$

In a single cantilevered beam scenario, the end of the beam can have a displacement and a slope. However, in a parallel beam scenario where the ends of the beams are fixed, the end of the beams may have displacement but must not have any slope. For a single

cantilevered beam with a force applied at the end, and the end constraint of zero slope applied, the Force/Deflection is Equation 2.

$$\frac{F}{\delta} = \frac{12EI}{L^3} \tag{2}$$

The stiffness is four times the stiffness of a standard cantilevered beam. With two beams, the resulting theoretical increase in stiffness of a dual parallel beam setup is eight times that of a single beam. Thus, a dual parallel beam configuration has a greater stiffness than the previously tested single beam configuration.

The parallel beam configuration can also support large loading in the vertical direction, and thus meets the third design goal. A robot equipped with a robot link of this design can be designed to have safety-related compliance in the horizontal axis without sacrificing the stiffness needed in the vertical axis to lift heavy loads.

A method to clamp two laminars in the parallel beam configuration was needed to construct the robot link. End clamps were designed and two were 3D printed from ABS. The end clamps are tightened via bolts to secure the two layer jamming laminars together in a parallel configuration. The assembly of the prototype robot link using two laminars and two end clamps can be seen in Figure 20.

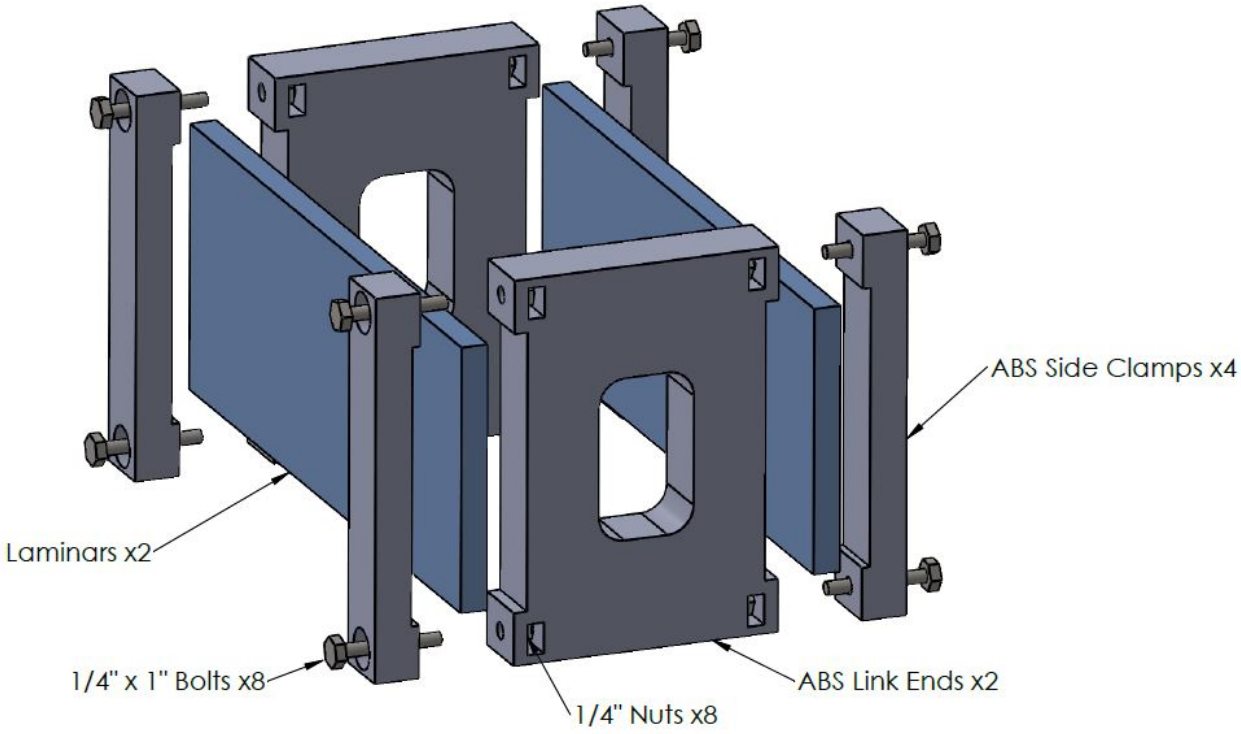

Figure 20: Prototype Link Design

This prototype link was designed to allow for easy for testing. The end clamps can accommodate laminar of thicknesses ranging from 5mm to 15mm, and with longer bolts can accommodate even wider laminars. The hole in the center of each Link End can be used to clamp the link to a table. The ends of the laminars are not obstructed by the clamps, so various methods of sealing the exterior vacuum bags can be used in conjunction with the clamps with no interference.

When fabricating this prototype link, several other modifications were made to the design of the laminar itself. The sharp corners of the center support were rounded for the prototype link. This reduces the risk of a corner of the ABS puncturing the sealed volume. Also, the three sealed sides of the volume were sealed using a heat sealer instead of a soldering iron. Instead of the silicon clamp, foil tape was used to seal the pneumatic hose

and the fourth side of the volume. This foil tape sealing method can be seen in Figure 21. It still allows for the layers within the laminars to be swapped as with the silicon clamp, but also provides a more robust seal.

Figure 21: Foil Tape Laminar Seal

Based on the results from the single beam tests, the robot link laminars used the 10mm center support and the interlocked layers configuration. As discussed in Chapter 3, this laminar configuration has a high maximum stiffness. Figure 22 shows the laminar configuration. The red areas of Figure 22 indicate the location of glue, which is necessary for the interlocked configuration. The blue exterior is the vacuum bag. The arrows indicate the force applied when negative pressure is applied to the laminar.

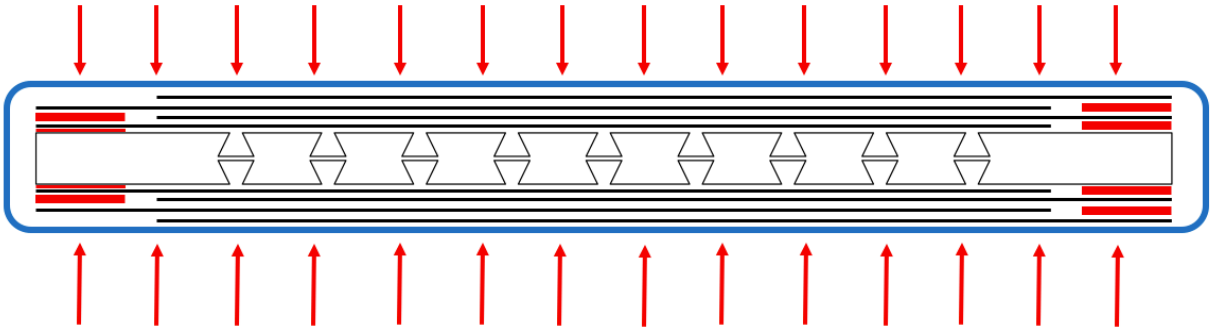

Figure 22: Laminar Configuration Used in Robot Link

4.2 Robot Link Analysis

Figure 23 shows the design of the 10mm center support used in the dual beam robot link. When in its minimum stiffness configuration, the stiffness contribution from the layers of the laminar is assumed to be negligible compared to the stiffness of the center support. Given this assumption, the robot link with zero applied pressure can be approximated using torsion springs and ridged bodies. Torsion springs are used to approximate the flexible sections of the center supports, while ridged bodies are used to approximate the ridged 10mm wide sections of the center supports. The model can be seen in Figure 24. The distance between the center of the two beams in the prototype and the model was 101.6 mm.

Equation 3 and 4 show the rotational spring constant calculation for a single .8mm wide flexible section of the beam. 1100 MPa and 2900 MPa are the minimum and maximum elastic modulus values for 3D printed ABS [15]. The wide variation of the elastic modulus values is caused by the variability of 3D printers, object orientation, and print

settings such as layer thickness and print temperature. The center supports were printed with the layers parallel to the beam and with 100% infill in the sections of the beam which bend, and as such should match the maximum elastic modulus value more closely.

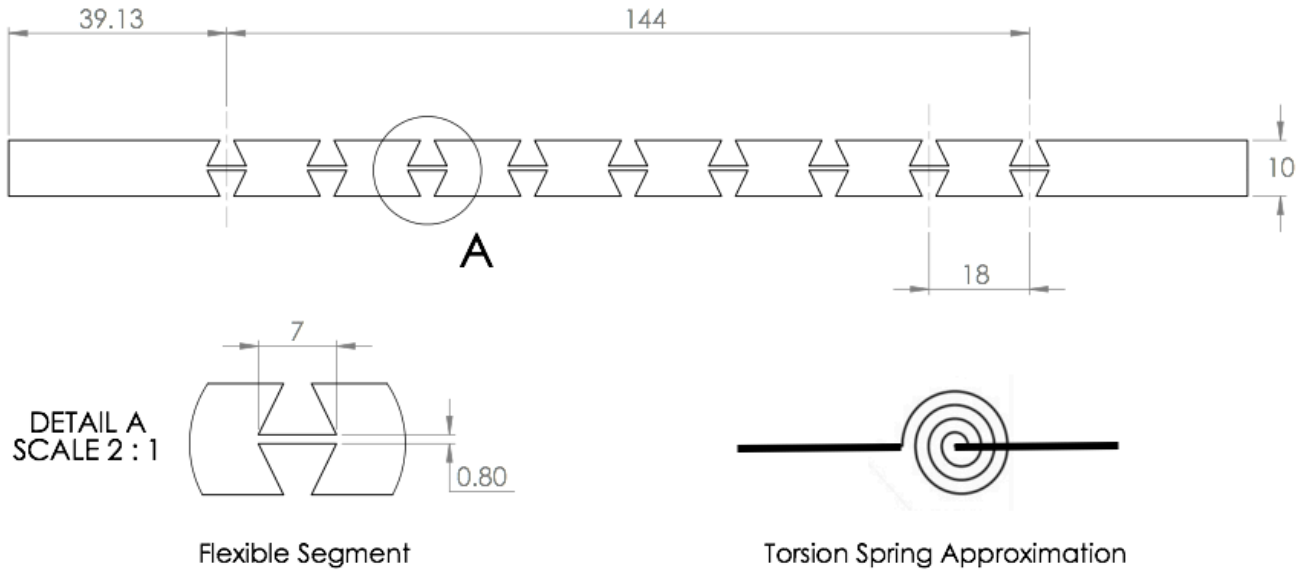

Figure 23: 10mm Center Support for Robot Link

$$K_{r\_min} = \frac{EI}{l} = \frac{E*\frac{1}{12}wh^3}{l} = \frac{1100MPa*\frac{1}{12}100mm*(.8mm)^3}{7mm} = 670.5 \text{ Nmm/rad} \quad (3)$$

$$K_{r\_max} = \frac{EI}{l} = \frac{E*\frac{1}{12}wh^3}{l} = \frac{2900MPa*\frac{1}{12}100mm*(.8mm)^3}{7mm} = 1767.6 \text{ Nmm/rad} \quad (4)$$

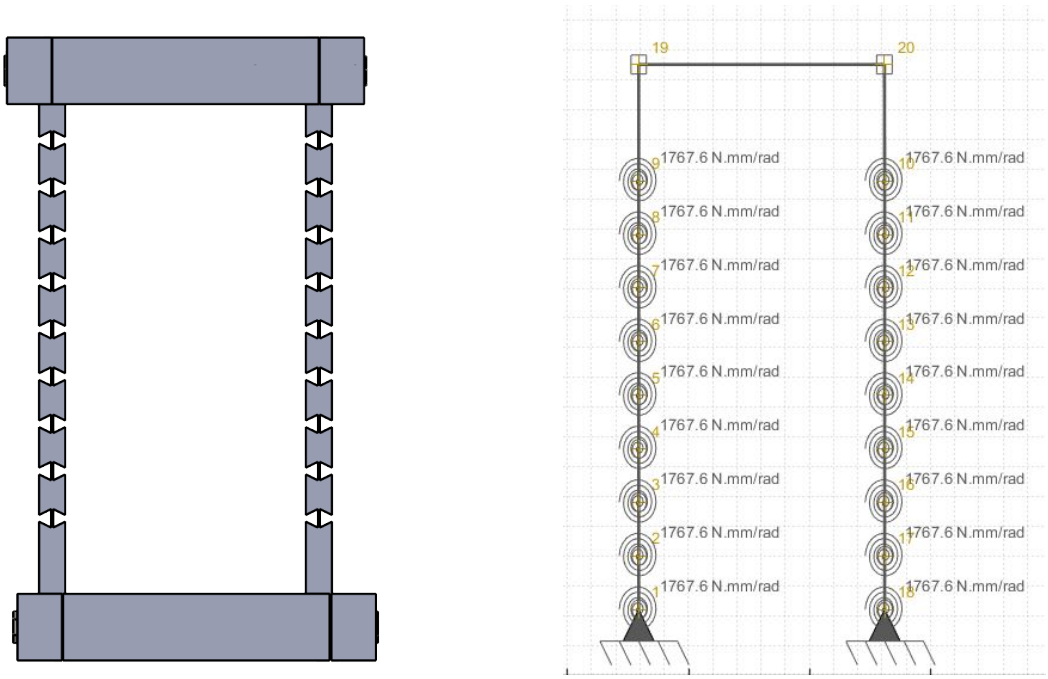

Figure 24: Robot Link vs. DAS-2D Model [16]

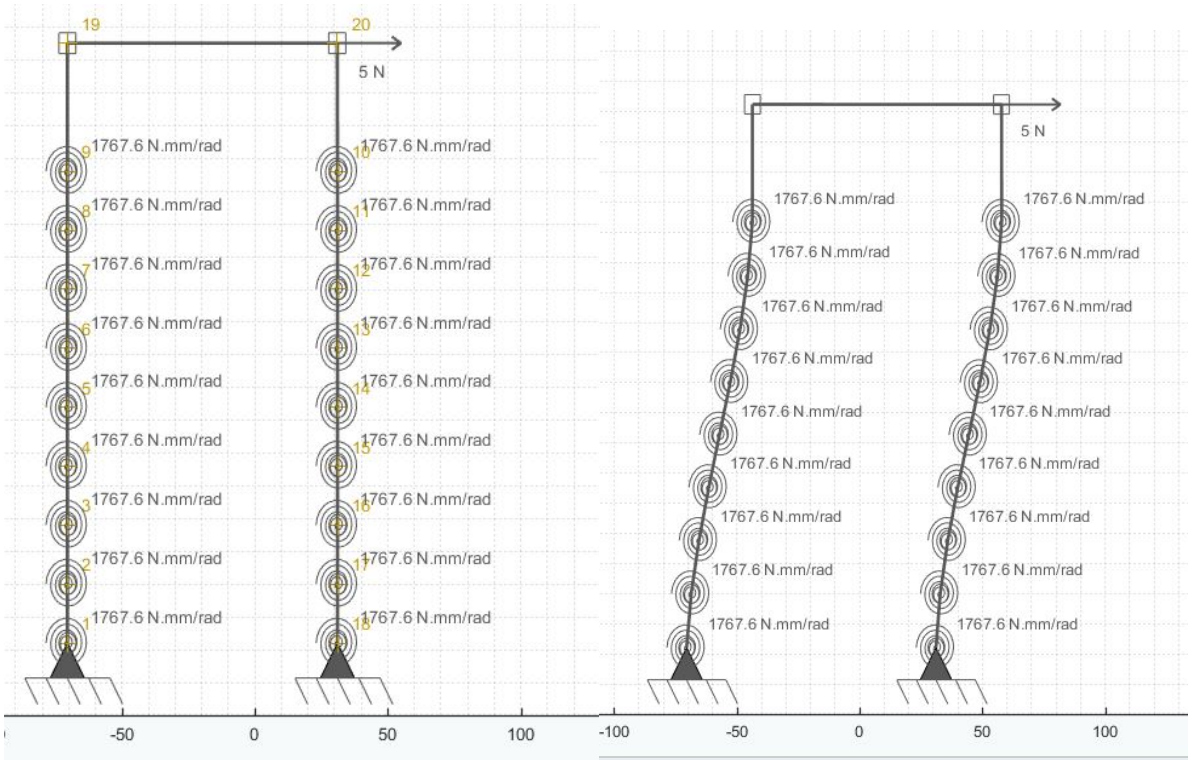

Figure 24: Deformation of Robot Link Using DAS-2D Simulation Software [16]

DAS-2D [16] was used to analyze the stiffness of the approximated robot link. A simulated load was applied to the model. The simulation was run using both 1100 MPa and 2900 MPa elastic modulus values. The resulting force vs. deflection curves can be seen in Figure 26. The deflection recorded was of the deflection in the X direction of point 20 in Figure 25.

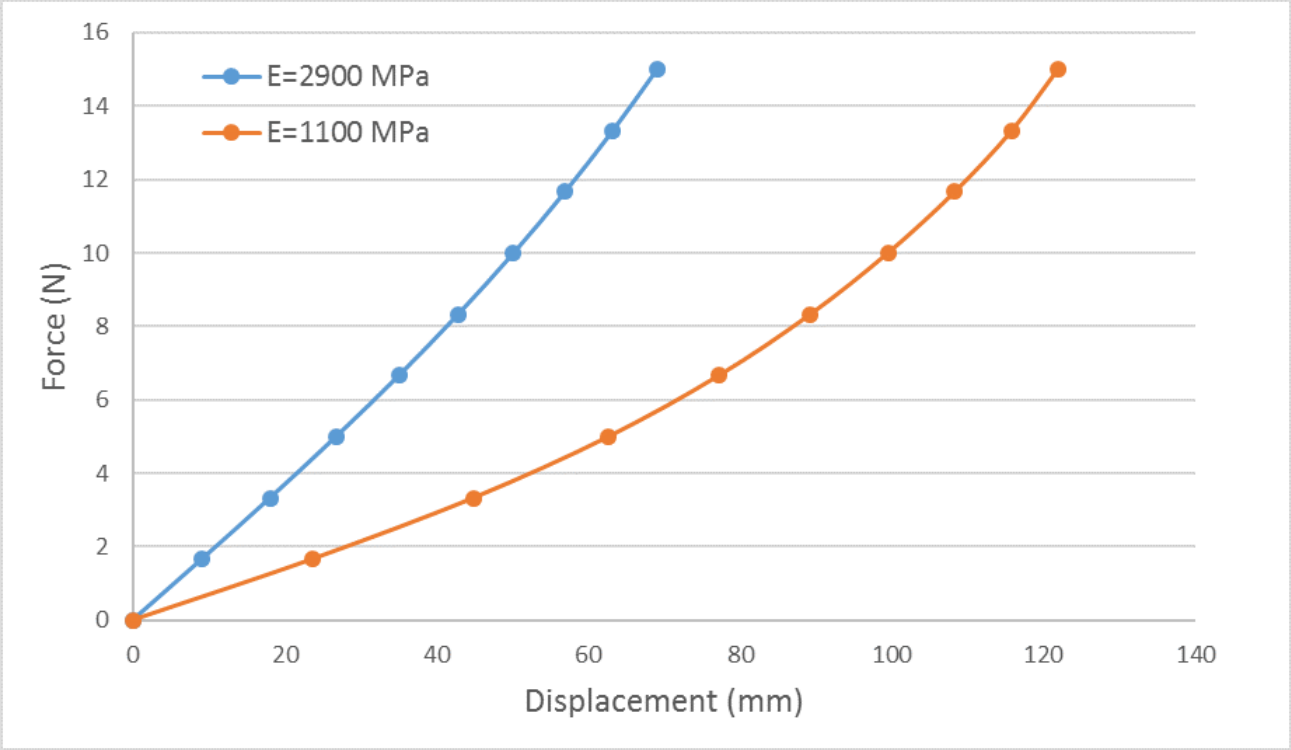

Figure 25: Simulated Minimum Stiffness Results of Robot Link

4.3 Robot Link Displacement Feedback Design

In robotic applications, it may be important to detect if deflection of the robot link has occurred. If deflection has occurred, the pressure of the link may need reduced to allow the link to self-center. Variable-resistance flex sensors were investigated as a method for detecting deflection of the link. 4.5 inch Spectra Symboflex flex sensors were tested with the prototype robot link. To measure the changes in resistance, one flex sensor was wired to an Arduino Uno as shown in Figure 27. The flex sensor was attached to the center support as shown in Figure 28. In this position, the sensor can be covered by the layers and the vacuum bag, and the two connecting wires can exit in the same location as the pneumatic tube. The layers and vacuum bag keep the sensor in position against the center support.

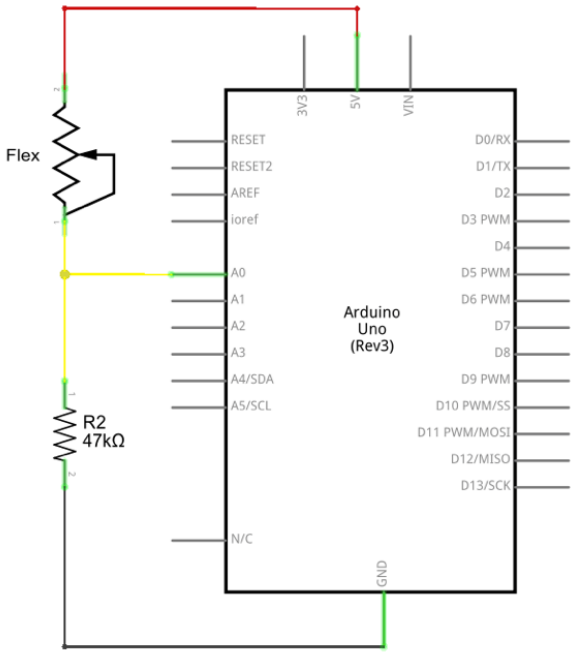

Figure 26: Flex Sensor Wiring Diagram [17]

Figure 27: Flex Sensor Placement

The Spectra flex sensors are directional, and are intended to detect bending in only one direction. For testing purposes, only one flex sensor was installed on the prototype robot link. For actual use, two flex sensors would be necessary if this model of flex sensor were used. For deflection detection in both directions, one flex sensor could be installed on either side of the robot link. Alternatively, the two flex sensors could be installed next to each other on one center support, with one sensor flipped 180 degrees about its length.

CHAPTER 5: ROBOT LINK TEST RESULTS

This chapter presents and discusses the testing of the prototype robot link. Section 5.1 describes the modifications that were made to the deflection test to accommodate the dual-beam robot link. Section 5.2 compares the minimum stiffness mode of the robot link to the analysis in Section 4.2. Section 5.3 compares the performance of the dual beam robot link to the single beam laminar evaluated in Chapter 3. Section 5.4 shows the force vs. deflection curves at different pressures for the different robot link configurations. The performance of the flex sensors for deflection detection is discussed in Section 5.5 Section 5.6 discusses the overall robot link performance and compares it to a mechanical linkage variable stiffness robot link.

5.1 Test Setup Modifications

The testing procedure for the dual beam prototype link was the same as the discussed in section 2.2 and used in the single beam deflection test. However, the dual beam robot link required several changes to the test setup. The Dyneema cord was replaced with a 28 gauge galvanized steel wire. The additional stiffness of the dual beam configuration made the Dyneema cord unsuitable. Also, the vice was replaced with a custom clamp constructed from wood, as seen in Figure 29. This custom clamp secured the link end at the top and bottom. There was no visible flexing of the link end during the stiffness test. Flexing at the link end would indicate compliance of the mount, which would interfere with the test results.

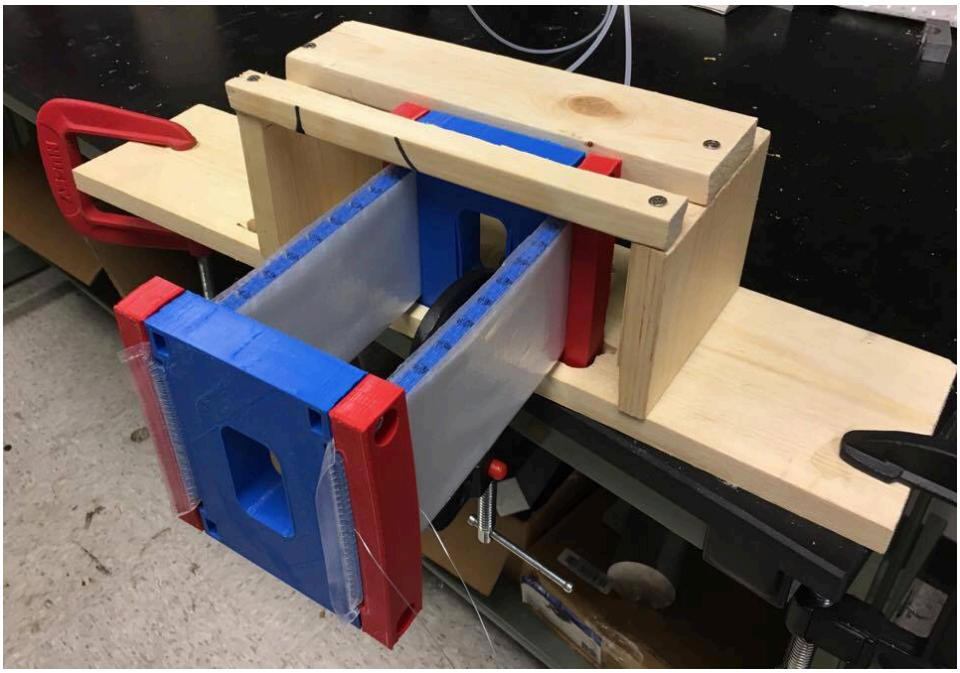

Figure 28: Robot Link Clamp

5.2 Comparison to Analysis

For the analysis of Section 4.2, the simplifying assumption was made that that the vacuum bag and layers did not contribute to the stiffness of the robot link when pressure was zero. To match this assumption, the robot link was first assembled with only the center supports of the laminars. A deflection test was done on this configuration. After this test, the robot link was assembled with eight layers per laminar and the vacuum bags. A deflection test was done using this configuration and with zero applied pressure.

Figure 30 shows the results of these two deflection tests compared to the theory values calculated in Section 4.2. With only the center supports, the robot link's deflection curve fell within the minimum and maximum deflection curves of Section 4.2. Thus, the experimental data agrees with the stiffness values calculated using DAS-2D.

The deflection test with the vacuum bag and the layers was stiffer than the test with the center support only. At 6mm of deflection, the deflection force was ~2.9 times greater for the robot link with the layers and the vacuum bag. At 12mm of deflection, the deflection force was ~2.6 times greater for the robot link with the layers and the vacuum bag. This suggests that the layers and vacuum bag significantly restrict the beam's deflection in the robot link's minimum stiffness mode. Tension was observed in the vacuum bag surface during the zero-pressure deflection. This tension may be one cause of the restricted motion when the robot link was configured with the layers and vacuum bag.

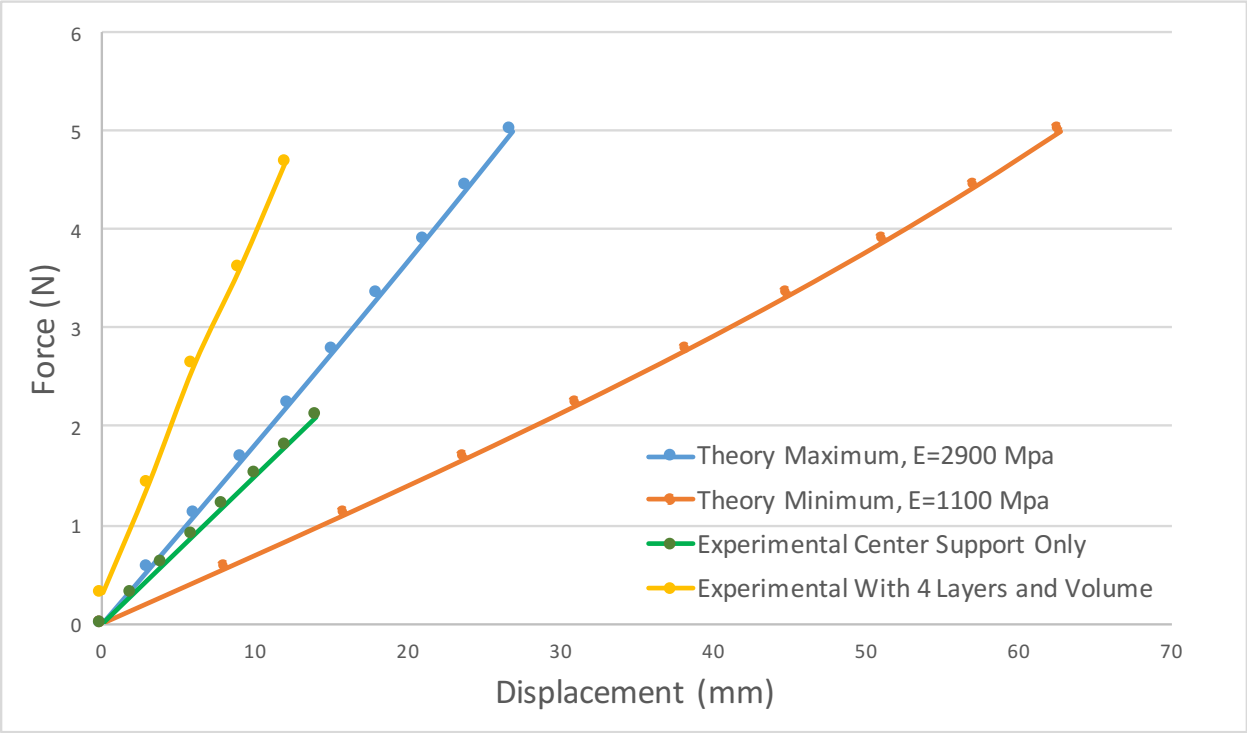

Figure 29: Minimum Stiffness of Robot Link vs. Analysis

5.3 Dual vs. Single Beam Study

The dual beam robot link was tested first with a 10mm center support and 8 sheets of Dura-lar polyester 0.005" matte film on each beam. The layers were in the interlocked configuration as described in Section 2.1. The results from this test were then compared to the single beam results of the same configuration as can be seen in Figure 31.

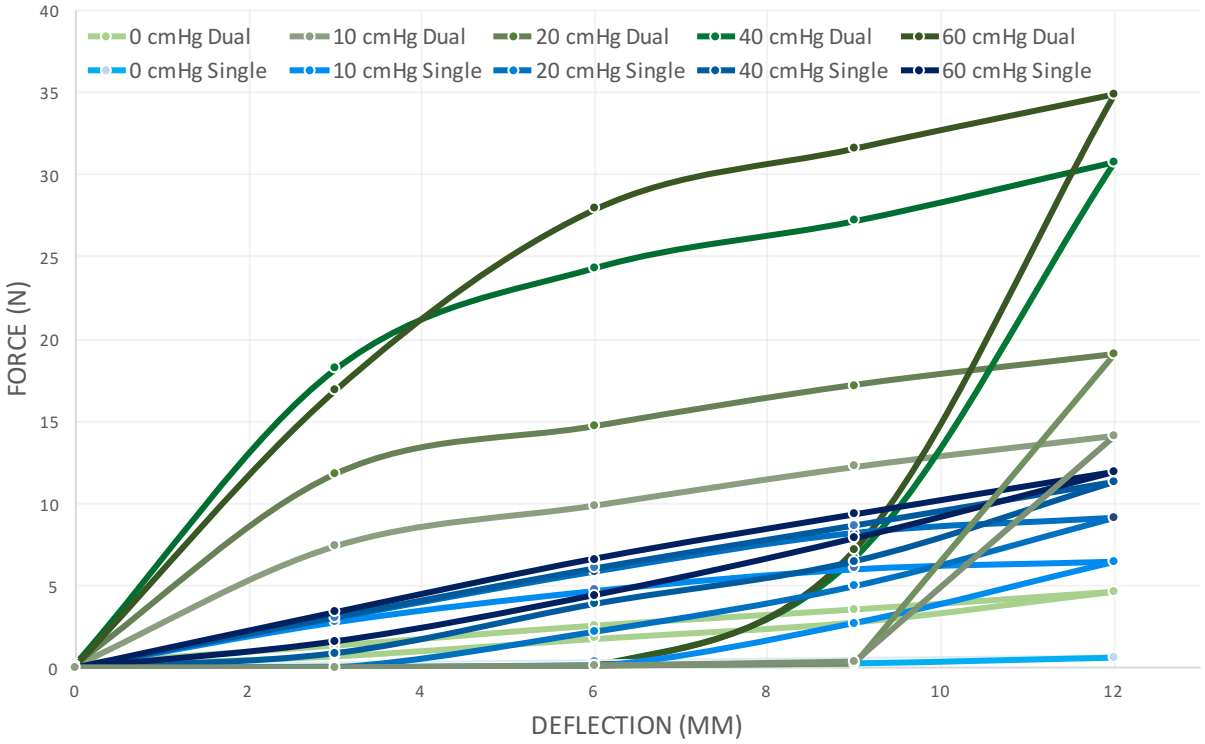

Figure 30: Single vs. Dual Beam Deflection Tests

The stiffness between zero and three millimeters of deflection was calculated for both the dual beam and the single beam configuration. This range was chosen to focus on the pre-slip stiffness of the laminars. Table 3 shows the results for 0, 20, 40, and 60 cmHg. These values from the layer jamming robot link do not match the 8 times stiffness increase that would be expected from a solid beam scenario, and the improvements in

stiffness seen with the dual beam configuration vary based on pressure. The zero-pressure test is closest to matching the theoretical 8 times stiffness increase, possibly because the laminar behaves most like a solid beam when the layer jamming effect is not activated.

Table 3: Single vs. Dual Beam Stiffness

Pressure (cmHg)	Stiffness Dual Beam ÷ Stiffness Single Beam
0	7.05
20	4.59
40	5.89
60	2.54

Slip between the layers happened sooner with the parallel beam configuration: ~3mm instead of ~15mm in the maximum stiffness configuration. However, the slip point was at a larger force with the parallel beam configuration: ~20N instead of ~15N with the maximum stiffness pressure. While less deflection was required before the layers began slipping in the parallel beam configuration, the force required for slip was greater. This, combined with the greater stiffness, suggests that the dual parallel beam configuration used in this prototype robot link will be better able to match the performance of rigid robots than the previously tested single beam configuration. The link will be able capable of larger loading and greater acceleration before slip occurs.

5.4 Dual Beam Pressure Tests

To determine the effect that the layer number had on the robot link's performance, deflection tests were run using 8, 12, 16, and 20 layers per beam. As with the other tests in this chapter, an interlocked configuration was used for the layers. The

results can be seen in Figures 32 through 35. When using 20 layers per beam, the force value exceeded the maximum reading of the force sensor. The cutoff of the force sensor is noted in Figure 35.

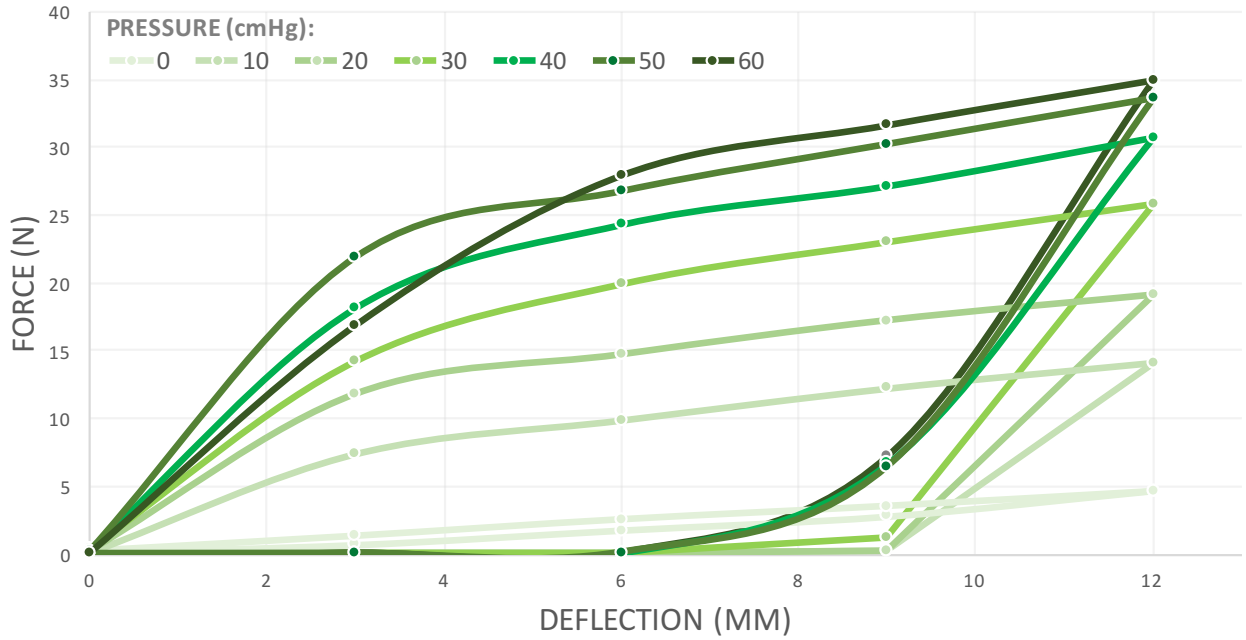

Figure 31: 8 Layers Per Beam Robot Link Pressure Test

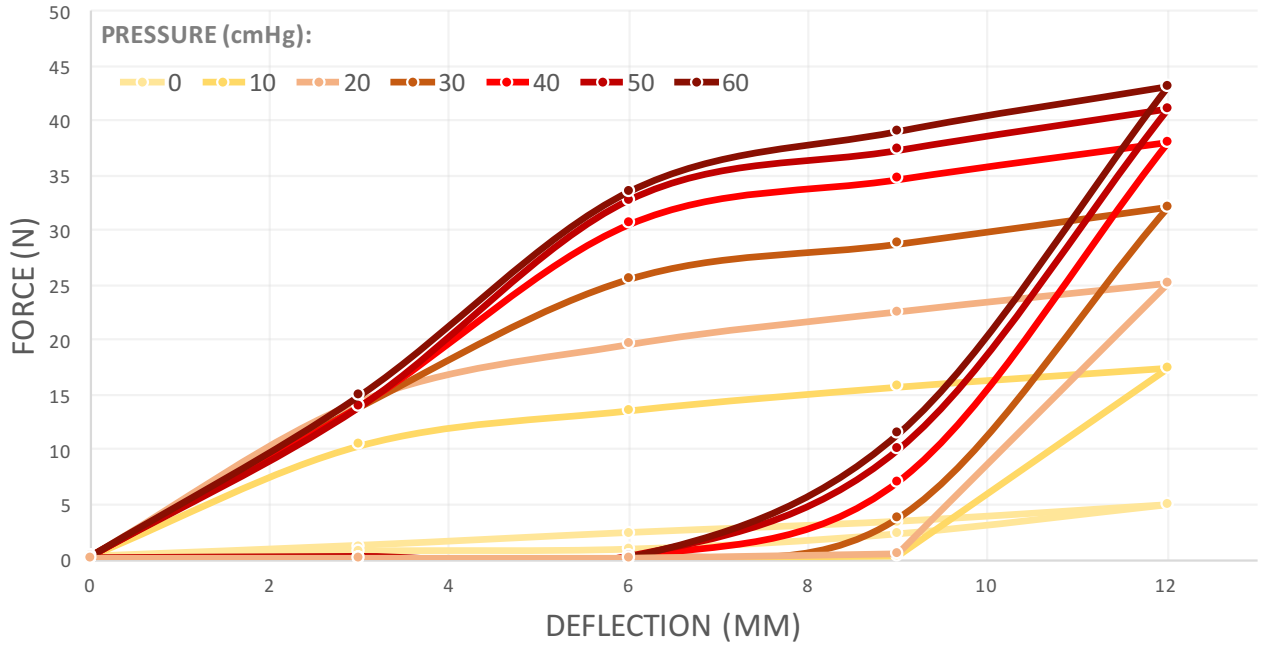

Figure 32: 12 Layers Per Beam Robot Link Pressure Test

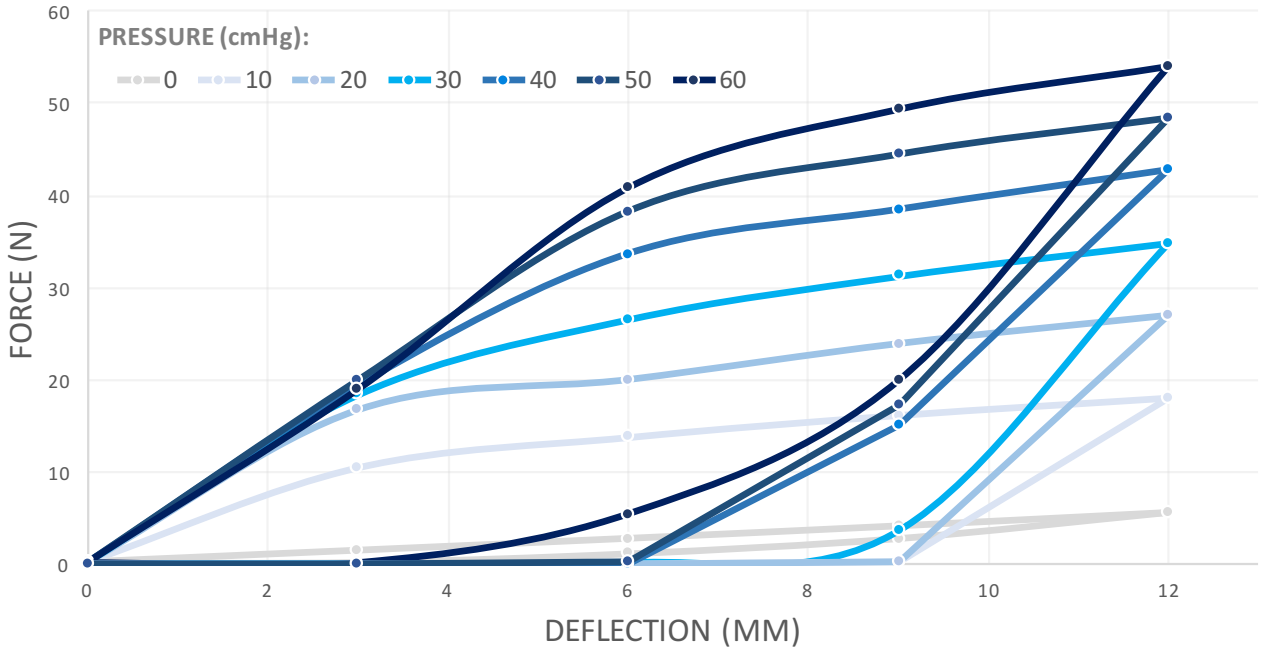

Figure 33: 16 Layers Per Beam Robot Link Pressure Test

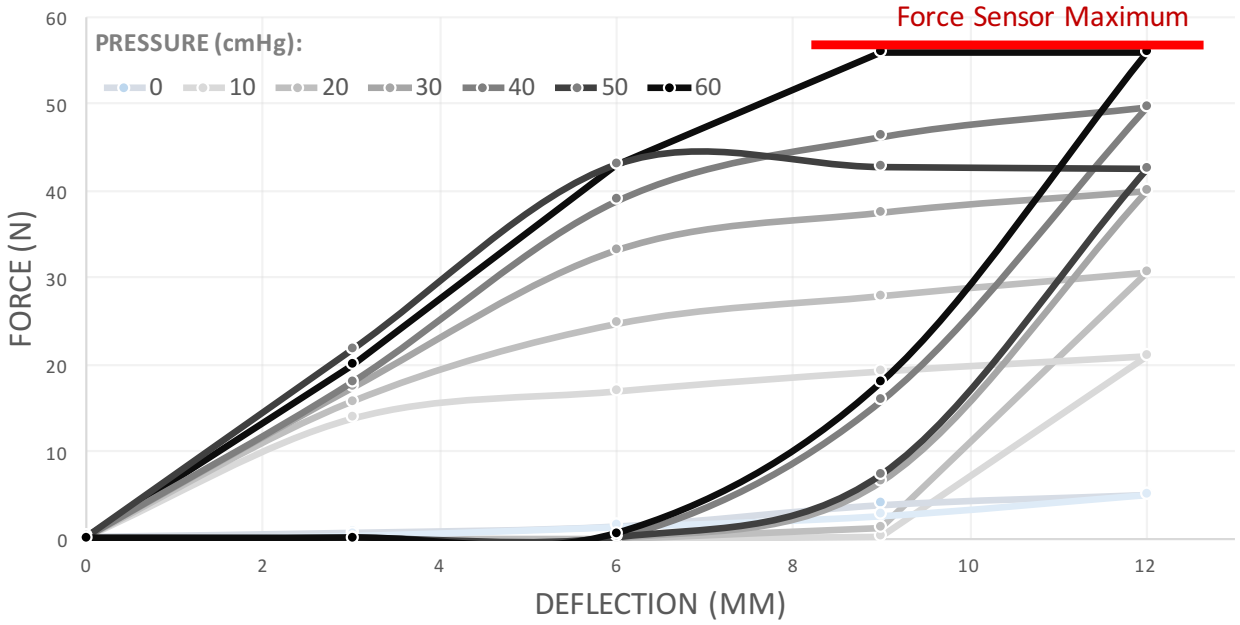

Figure 34: 20 Layers Per Beam Robot Link Pressure Test

Figure 36 through 38 can be used to compare the different numbers of layers. The additional number of layers did not affect the stiffness significantly in the minimum stiffness configuration, as the layers were not jammed when the pressure was zero. Also, the additional layers did not have a large effect on the stiffness of the laminar before slip occurs. The additional layers did, however, increase the force at which slip was observed.

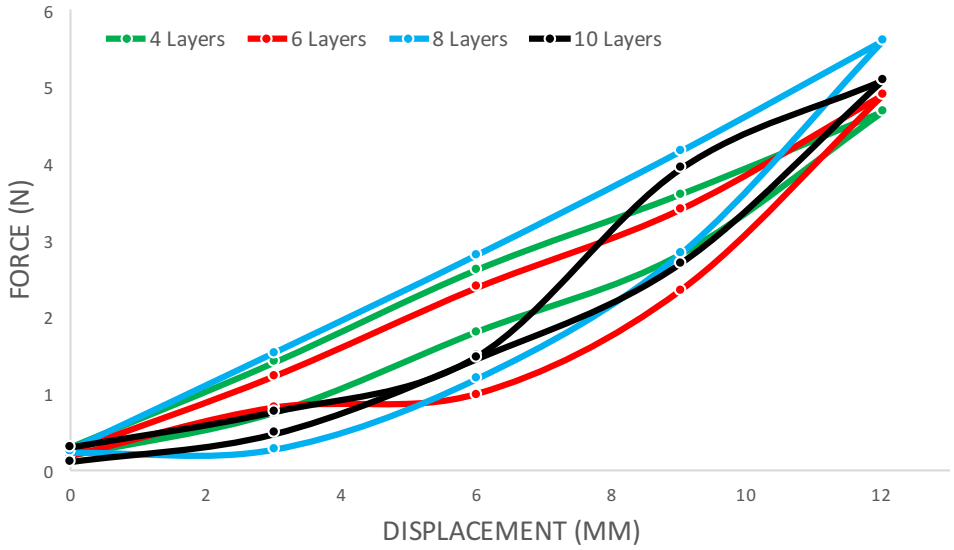

Figure 35: Layer Number Comparison ocmHg

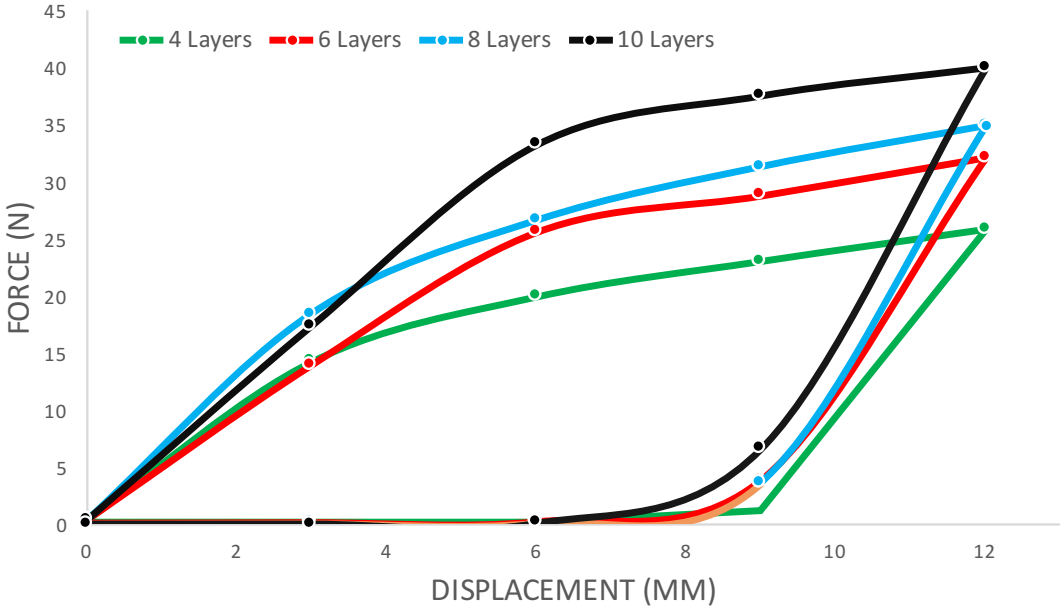

Figure 36: Layer Number Comparison 30 cmHg

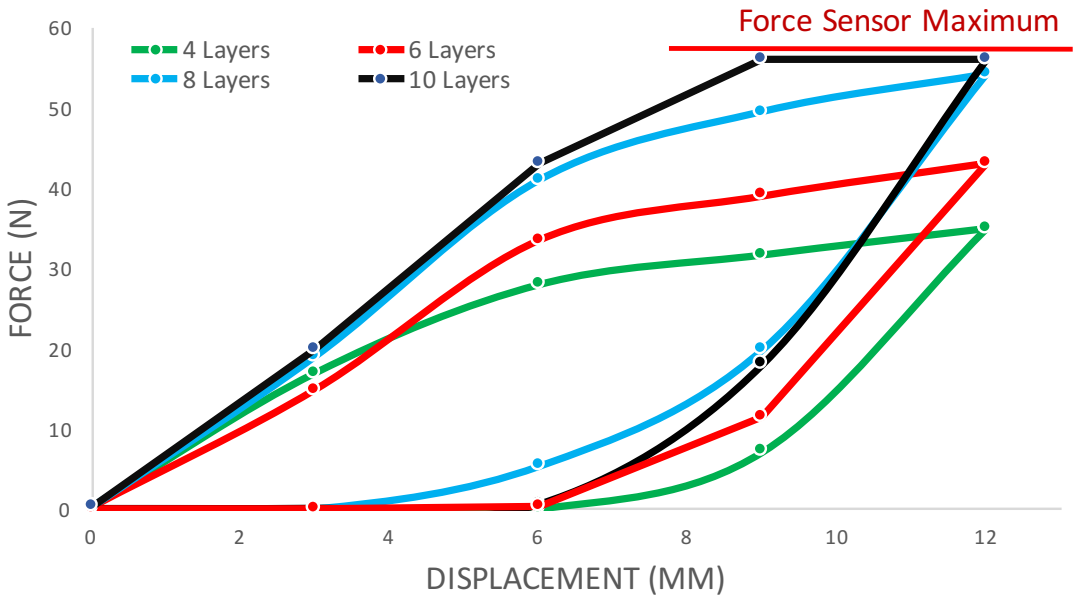

Figure 37: Layer Number Comparison 60 cmHg

As can be seen in Figure 38, the slip point occurs around 6 mm of deflection when ten layers per beam was used, while the slip point occurs earlier around 3mm when only four layers were used. The stiffness at 60 cmHg with ten layers per beam was the greatest of any configuration tested. Three tests of this configuration were performed, and the average force recorded at 6mm of deflection was 43.66N, which is a stiffness of 7.27 N/mm. The stiffness between 0 and 6mm for this configuration of the robot link at 0 cmHg was 0.46 N/mm. The total change in stiffness for this configuration of the beam was 15.8 times, which is the greatest of the tested configurations.

Table 4 and Table 5 summarize the pressure tests performed on the robot link. The stiffness values reported in Table 4 are from 0mm to 3mm of deflection, as this was before the slip point of all the trials. In Table 5, the deflection force for 10 sheets at 60 cmHg is

unknown but greater than 55.83 N, because the recorded value was above the reading limit of the force sensor.

Table 4: Robot Link Stiffness vs. Layer Number

Initial Robot Link Stiffness from 0 to 3mm Deflection (N/mm)							
	Pressure (cmHg)						
Layer Number Per Beam	**0**	**10**	**20**	**30**	**40**	**50**	**60**
4	0.37	2.42	3.84	4.60	5.96	6.88	5.58
6	0.33	3.36	4.71	4.53	4.58	4.55	4.66
8	0.42	3.42	5.49	6.05	6.40	6.57	6.26
10	0.15	4.53	5.17	5.69	5.92	7.14	7.07

Table 5: Robot Link Deflection Force vs. Layer Number

Force at 12mm Deflection							
	Pressure (cmHg)						
Layer Number Per Beam	**0**	**10**	**20**	**30**	**40**	**50**	**60**
4	4.68	14.13	18.93	25.80	30.78	33.65	34.65
6	4.90	17.50	25.19	32.10	38.10	41.08	43.50
8	5.60	18.10	27.02	34.88	42.80	48.40	54.09
10	5.09	21.06	30.61	40.00	49.71	42.50	>55.83

5.5 Displacement Feedback Test

To determine if the flex sensor could accurately detect deflection of the robot link, the link was deflected to 25.4mm and the resistance values were measured by the Arduino at four deflection increments. This deflection test was conducted five times to check the variation of the sensor. Between each deflection test the robot link was deflected back and forth several times between 25.4mm and negative 25.4mm to mimic the deflection

that might be seen in use over time. Figure 39 shows the average resistance values of the flex sensor vs. the deflection amount. The error bars on Figure 39 show the variation seen in the values.

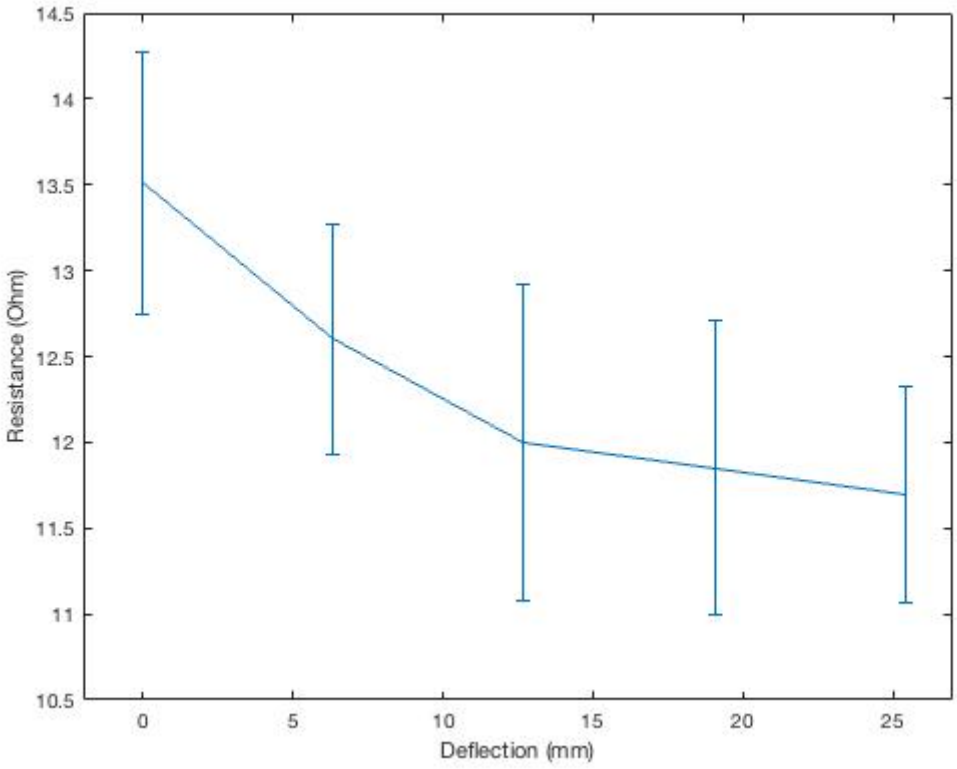

Figure 38: Flex Sensor Position Data

The flex sensor was capable of detecting deflection of the robot link. However, because of the variation seen in the flex sensor resistance values, the sensor can only reliably detect larger deflections. The standard deviation of the zero-deflection resistance was .66 Ohms. The average difference in resistance when the link was deflected 25.4mm was 1.8 Ohms. A displacement feedback method capable of detecting smaller displacements with greater certainty is still needed.

5.6 Conclusion of the Prototype Robot Link Design

The dual beam configuration combined with the 10mm wide center supports produces stiffness values which are greater than those found in other layer jamming research. Additionally, the stiffness change achieved is greater than the mechanically actuated variable stiffness robot link which was designed at the DISL, as can be seen in Table 6. The stiffness change achieved by the mechanically actuated robot link was 3.6 times, while the layer jamming robot link achieved a stiffness change of 15.8 times [14]. This is the result of the maximum stiffness of the layer jamming robot link being greater than that of the mechanically actuated robot beam. The minimum stiffness values are comparable. Table 6 compares the layer jamming robot link to just one configuration of mechanically actuated robot link, and it must be noted that other configurations of mechanical actuation may perform differently.

Table 6: Layer Jamming vs. Mechanical Actuation

	Layer Jamming	Mechanical Actuation [14]
Minimum Stiffness (N/mm)	0.46	0.54
Maximum Stiffness (N/mm)	7.27	1.936
Stiffness Change	15.8	3.6

CHAPTER 6: CONCLUSION

5.1 Contributions

This thesis applies the variable stiffness properties of layer jamming to a new application and presents a laminar design with a center support that greatly increases maximum stiffness. Previous layer jamming research has focused on flexible displays, clothing, small robotic grippers, and other highly compliant applications that do not attempt to achieve stiffness levels comparable to ridged robots. The variable stiffness robot link application discussed in this thesis requires a greater stiffness than many past layer jamming applications. A novel laminar configuration was used to achieve this greater stiffness capability.

The use of a center support is a new approach to layer jamming laminars. The center support spaces the layers, and the friction forces associated with them, away from the center of the laminar. This approach increases the moments caused by the friction forces, allowing the beam to better resist bending moments in the maximum stiffness configuration. This thesis demonstrates that greater stiffness values are possible when the center support is utilized. The center support also adds self-centering capabilities to the laminar, which is important in applications that require accurate positioning. The new laminar configuration investigated in this thesis expands the possibilities of layer jamming to applications which require stiffness and self-centering capabilities not possible with other laminar configurations.

Another contribution of this thesis is the dual beam configuration of the robot link. The dual beam configuration has been used in conjunction with other variable

stiffness technologies, but not layer jamming. The dual beam configuration combined with the center supports of the laminar constrains the compliance to just one dimension. This allows the robot link to withstand higher loads in the non-compliant directions. Other layer jamming configurations are compliant in greater than one dimension, which reduces their load-carrying capabilities. Combined with the center support, the dual beam configuration also increases the stiffness values possible with layer jamming.

5.2 Future Work

The performance of the robot link in this thesis could be improved further. The number of layers of the robot link was varied, but there are other variables to be investigated in the future. Different center support widths, laminar sizes, layer materials, and numbers of parallel beams should be investigated.

Additionally, efforts could be made to improve the ease of manufacturing. The current configuration uses two separate vacuum bags for the two laminars. The possibility of combining these into a single volume should be explored. Additionally, other materials and configurations should be explored for the exterior volume. The volume could potentially be created using the outermost layers as two of the walls, which a seal going around the edge of the laminar connecting the outermost left layer to the outermost right.

Improvements can be made to the deflection detection method. The tested flex sensors were not as precise as would be ideal. Multiple flex sensors could be used and their results averaged to increase the certainty of the measured deflection amount. The

flex sensor could also be mounted in the center of the center support, instead of along the side, for better packaging. Alternatives to flex sensors should also be investigated.

5.3 Summary

A variable-stiffness robotic arm link utilizing layer jamming technology was designed and tested. The goal of this robot link was to achieve the precision and load capabilities of a traditional robot with the safety of a compliant soft robot. Laminar samples of various designs were tested, and positive relationship between number of layers and maximum stiffness was observed. A wide center support was found to greatly increase the maximum stiffness of the laminar. A configuration with a high maximum stiffness was selected to give the robotic arm high load capabilities, and a prototype arm link was built and evaluated.

BIBLIOGRAPHY

[1] Antonio Bicchi and Giovanni Toniettif. Fast and "Soft-Arm" Tactics. In *IEEE Transactions on Robotics,* June 2004

[2] Bryan E. Schubert and Dario Floreano. Variable stiffness material based on rigid low-melting-point-alloy-microstructures embedded in soft poly(dimethylsiloxane) (PDMS). In *RSC Advances*, Oct 2013.

[3] Daniela Rus and Michael T. Tolley. Design, fabrication and control of soft robots. In *Nature,* May 2015

[4] Deepak Trivedi et al. Soft robotics: Biological inspiration, state of the art, and future research. In *Applied Bionics and Biomechanics,* September 2008.

[5] E. Steltz et al. JSEL: Jamming Skin Enabled Locomotion. In *IEEE/RSJ International Conference on Intelligent Robots and Systems*, 2009

[6] Eric Brown et al. Universal robotic gripper based on the jamming of granular material. In *PNAS*, September 2010.

[7] G. J. Liao et al. Development of a real-time tunable stiffness and damping vibration isolator based on magnetorheological elastomer. In *Journal of Intelligent Material Systems and Structures*, 2011

[8] H. Nakai et al. Metamorphic robot made of low melting point alloy. In *IEEE/RSJ International Conference on Intelligent Robots and System*, 2002

[9] Hua-xia Deng et al. Development of an adaptive tuned vibration absorber with magnetorheological elastomer. In *Institute of Physics Publishing, Smart Materials and Structures*, 2006

[10] Jifei Ou et al. jamSheets: Thin interfaces with tunable stiffness enabled by layer jamming. In *Proceedings of the 8th International Conference on Tangible, Embedded and Embodied Interaction*, 65-72, 2014.

[11] N. E. Brown et al. Universal robotic gripper based on the jamming of granular material. In *National Academy of Sciences, USA*, vol. 107, 2010.

[12] Wood RJ and Walsh CJ. Smaller, softer, safer, smarter robots. In *Science Translational Medicine*, May 2013.

[13] Yong-Jae Kim et al. A novel layer jamming mechanism with tunable stiffness capability for minimally invasive surgery. In *IEEE Transactions on Robotics,* article has been accepted for inclusion in a future issue of this journal.

[14] Yu She, Hai-Jun Su, et al. Design and Prototype of a Tunable Stiffness Arm for Safe Human-Robot. In *ASME 2016 International Design Engineering Technical Conference,* August 2016.

[15] The Difference Between ABS and PLA for 3D Printing, Online at http://2015.igem.org/wiki/images/2/24/CamJIC-Specs-Strength.pdf. 2013.

[16] Design, Innovation and Simulation Lab of Ohio State University. DAS 2D/3D. Online at http://compliantanalysis.com/. 2017.

[17] Flex Sensor Hookup Guide. Online at https://learn.sparkfun.com/tutorials/flex-sensor-hookup-guide